Heat transfer within mortar containing micro-encapsulated PCM: Numerical approach

A. El Ouali, T. El Rhafiki, Tarik Kousksou, A. Allouhi, M. Mahdaoui, A. Jamil, Youssef Zeraouli

Heat transfer within mortar containing micro-encapsulated PCM: Numerical Approach

M. Elouali[(a)], T. El Rhafiki[(a)] , T. Kousksou[(b)] , A. Allouhi[(c)], M. Mahdaoui[(d)], A. Jamil[(c)], Y. Zeraouli[(b)]

[(a)] Ecole Nationale Supérieure d'Arts et Métiers, ENSAM Marjane II, BP - 4024 Meknès Ismailia, Maroc

[(b)]UNIV PAU & PAYS ADOUR/ E2S UPPA, Laboratoire des Sciences de l'Ingénieur Appliquées à la Mécanique et au Génie Electrique – Fédération IPRA, EA4581, 64000, PAU, FRANCE

[(c)]Université Sidi Mohamed Ibn Abdelah, École Supérieure de Technologie de Fès, Route d'Imouzzer BP 2427, Maroc.

[(d)]Equipe de Recherche en Transferts Thermiques & Énergétique - UAE/E14FST Département de Physique FST, Université Abdelmalek Essaâdi Tanger - Maroc

Abstract: An axisymmetric physical model based on the porous medium approach was performed to quantify the thermal gradients inside a building material containing microencapsulated phase change material (PCM) in the differential scanning calorimeter cells. The conservation equations are solved numerically using finite difference method. The general expressions of the specific enthalpy, the apparent heat capacity and the equivalent heat capacity are exposed. The influence of various parameters like the heating/cooling rate, the volume fraction of the PCM and the sample masse on the thermal behavior of these materials is investigated and discussed. Despite the small dimensions of the differential scanning calorimeter samples, important temperature gradients were observed during the phase change process of the PCM.

Keywords: Microencapsulated PCM, Heat transfer, Building, DSC, Hysteresis phenomenon.

Nomenclature

a Superficial capsule area per unit bed volume (m^{-1})

c Specific heat ($J\,kg^{-1}\,K^{-1}$)

d Diameter (m)

f PCM liquid mass fraction

h Specific enthalpy ($J.\mathrm{kg}^{-1}$)

k Heat conductivity ($W\,m^{-1}\,K^{-1}$)

K Heat transfer coefficient, ($\mathrm{W.m^{-2}.K^{-1}}$)

L_f Latent heat of PCM ($J\,kg^{-1}$)

M Mass, (kg)

r Radial coordinate (m)

t Time (s)

T Temperature (K)

U Heat transfer coefficient, ($\mathrm{W.m^{-2}.K^{-1}}$)

Z Space variable, (m)

Greek symbols

β Heating/cooling rate ($°C\,min^{-1}$)

ΔS surface (m^2)

ε Porosity

λ Heat conductivity ($W\,m^{-1}\,K^{-1}$)

Φ Heat flow rate ($W\,g^{-1}$)

Subscripts, superscripts

B Building material

eq Equivalent

Liq Liquid

m Melting

i Initial

P Plate temperature

pcm Phase change material

sol Solid

1. Introduction

The incorporation of phase change material (PCM) into conventional building materials is currently designed as an efficient solution to ameliorate the thermal inertia of the building [1-3]. Various techniques can be used to incorporate the PCM into conventional materials: direct integration, immersion, micro-encapsulations or macro-encapsulations [4-6]. In microencapsulation technique, the PCM is included within a microscale polymeric-head [7-12]. During the phase change process, the microencapsulation technique allows to keep the liquid PCM within conventional building materials by eliminating the dependence on capillarity phenomenon [12].

It is interesting to recall that the knowledge of the thermophysical properties of PCM like heat capacity, thermal conductivity, phase change temperatures and enthalpy, is very important to design and optimize micro-encapsulated PCM in building envelope systems [13-15]. Moreover, accurate estimation of these properties during the phase change process is essential for correct physical modeling of the micro-encapsulated PCM.

Many studies have been conducted to determine experimentally the thermophysical properties of the micro-encapsulated PCM in the building envelope systems [10-12].Thermal analysis methods are usually used to characterize PCM [16-20]. Among these methods, differential scanning calorimetry (DSC) is one of the most-commonly used technique for determining the thermophysical properties of PCMs [19-20]. The DSC methods consider isothermal conditions to be inside the sample and this condition restricts the samples to very small sizes (1-10 mg), which may cause the thermo-physical properties of the test sample to be different from those of the bulk product [20]. High heating and cooling rates can cause temperature gradients inside the PCM test sample and can generate measurement errors [21-23].

Numerical simulations are also performed to investigate PCM-based systems [24-27]. Such simulations will not be reasonable if the PCM data is not relating its performance in a correct way, so also for this reason reliable and credible results from the characterization are required.

In this paper, a physical model is performed and developed in order to quantify the thermal behavior of microencapsulated PCM incorporated in building material and to help users of power compensation DSC device to better interpret the curves and the results obtained by this apparatus. Finally, we present some guidelines to understand some phenomena during the phase transition process inside materials containing microencapsulated PCM and to avoid any possible errors during the use of the DSC apparatus.

2. Differential Scanning Calorimeter

Differential Scanning Calorimetry (DSC) is the most popular measurement technique for detecting endothermic (melting) and exothermic (freezing) transitions such as the determination of the melting temperature and the enthalpy of the PCM during the melting/freezing process. In power compensation DSC the active (sample) and reference cells are placed in disconnected furnaces, which are both imposed to the same temperature (see **Fig.1**). The eventual difference in heat flow-rate between the furnaces is electrically compensated.

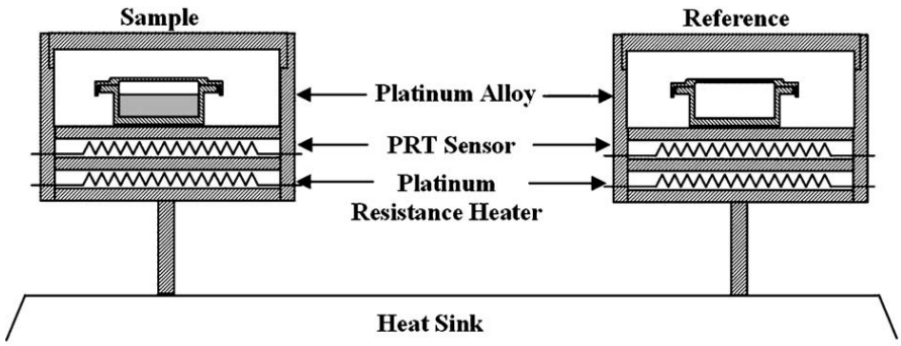

Fig.1: Scheme of the head of the DSC

In power compensation DSC, the flow-rate Φ needed, to maintain the reference material and the test sample at the same plate temperature $\mathbf{T_p}$ of the metallic crucibles, is recorded during time:

$$\Phi = \Phi_{active\ cell} - \Phi_{reference\ cell} \quad \textbf{(1)}$$

As pointed out in Ref **[28-31],** the heat flow rate restituted by the reference crucible is approximately constant and equal to $\Phi_{ref} = \beta.c_R$, β is the heating/cooling rate and c_R is the specific heat capacity of the reference cell. So, to facilitate the physical model, the heat flow rate exchanged at the reference crucible is neglected from the calculation of Φ (equivalent to the shift in the baseline).

3. Physical model

The microencapsulated PCM incorporated in the cement mortar is placed in the active cell (**Fig.2**). The thermophysical properties of cement mortar and PCM are indicated in **Table 1-a and Table 1-b [11].**

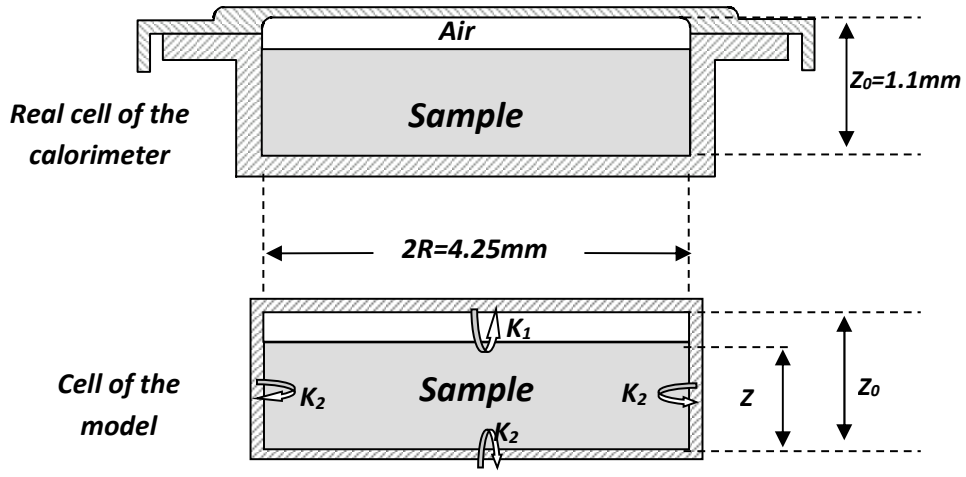

Fig.2: Scheme of the DSC cell

Table 1-a: Physical Properties of Mortar

Density	1400 $kg.m^{-3}$
Thermal conductivity	0.65 $W.m^{-1}.°C^{-1}$
Specific heat capacity	925 $J.kg^{-1}°C^{-1}$

Table 1-b: Physical Properties of PCM

Density (solid/liquid)	995 $kg.m^{-3}$
Thermal conductivity (solid)	0.2 $W.m^{-1}.°C^{-1}$
Thermal conductivity (liquid)	0.13 $W.m^{-1}.°C^{-1}$
Specific heat capacity (solid)	1700 $J.kg^{-1}°C^{-1}$
Specific heat capacity (liquid)	2153 $J.kg^{-1}°C^{-1}$
Latent heat of fusion	16674$J.kg^{-1}$
Melting temperature	26 °C

The micro-encapsulated PCM diameter is estimated to be $100\mu m$ **[11].**The shape of the active cell is supposed to be cylindrical and their dimensions are $2R_0 = 4.25mm$ for the diameter and $Z = 0.82\,mm$ for the height of the building material (see **Fig.2**). Each face of the active cell (see **Fig.2**) is exposed to a time dependent linear plate temperature:

$$T_p = \beta.t + T_0 \qquad \textbf{(2)}$$

Where β is the heating/cooling rate and T_o the temperature of the sample at t = 0.

The linear variation of the plate temperature enables us to comfortably identify any deviation on the sample temperature provoked by the heat transfer and the phase change inside the sample.

Generally, detailed modeling of the heat transfer inside composite material containing is quite complex. The complexity of the problem resides in two aspects:

- The definition of the appropriate expression for energy stored during the phase change process of the PCM in the building material.
- The combination of two physical phenomena in the same environment: heat transfer in porous media and thermal behavior of phase change material encapsulated in the mortar.

To reduce the complexity of this problem, we have assumed the following assumptions.

- The DSC sample geometry is cylindrical.
- Heat transfer inside the mortar is generated by heat conduction in two-dimensions (r and z).
- Thermal gradients inside microencapsulated PCM are neglected.
- The intra-microcapsules temperature gradients are neglected.
- The fusion and freezing operations occur at an identical temperature (T_m = 26°C).
- The thermophysical properties of the building material are not dependent on temperature,
- The thermophysical properties of the PCM are different for the solid and liquid phases.

In this study, the mortar containing microencapsulated PCM is regarded as a porous medium. The governing equations for heat transfer inside the building material are determined by assuming a representative elementary volume (VER) including mortar and microencapsulated PCM with volume fractions $(1-\varepsilon)$ and ε. The heat transfer across a porous medium can be investigated using energy equation. This equation can be described for two conditions involving local thermal equilibrium and non-local thermal equilibrium.

For local thermal equilibrium, the thermal gradient at any point between the two phases: mortar and microencapsulated PCM is supposed to be negligible.

$$(\rho c)_{pr}\frac{\partial T_{pr}}{\partial t}=k_{pr}\left(\frac{\partial^2 T_{pr}}{\partial r^2}+\frac{1}{r}\frac{\partial T_{pr}}{\partial r}+\frac{\partial^2 T_{pr}}{\partial z^2}\right)-\rho_{pcm}L_f\,\varepsilon\frac{\partial f}{\partial t} \quad \textbf{(1)}$$

where $(\rho c)_{pr}$ and k_{pr} are the total heat capacity per volume and the thermal conductivity of the porous medium, respectively. These parameters can be calculated using the following expressions:

$$(\rho c)_{pr}=(1-\varepsilon)(\rho c)_B+\varepsilon(\rho c)_{pcm} \quad \textbf{(2)}$$

$$(\rho c)_{pcm}=f.(\rho c)_{pcm,l}+(1-f).(\rho c)_{pcm,s} \quad \textbf{(3)}$$

$$k_{pr}=(1-\varepsilon)k_B+\varepsilon k_{pcm} \quad \textbf{(4)}$$

$$k_{pcm}=f\,k_{pcm,l}+(1-f)k_{pcm,s} \quad \textbf{(5)}$$

where subscripts *B* and *pcm* refer to the building material and phase change material phases, respectively.

The left hand side of **Eq.(1)** denotes the rate of change of the enthalpy of the porous medium in the VER. The first term on the right hand side indicates the heat exchanged by conduction in the axial and radial directions of the control volume. The evolution of the latent heat during the phase change process of the PCM is accounted by using the source term $\rho_{pcm}L_f\varepsilon\frac{\partial f}{\partial t}$ in **Eq.(1)**, where f is the liquid fraction of PCM undergoing phase change and L_f is the latent heat of fusion of the PCM. The value of f is related to the temperature T_{pr} and determines the rate of evolution of latent heat during phase change process. The liquid fraction f takes the value 1 for fully liquid control volume and 0 for fully solid control volume. Its value lies in the interval $]0,1[$ for the control volumes in which the PCM exist at the liquid and solid phases.

The use of the local thermal equilibrium approach is not widely used to describe the phase change process inside the composite material because the assumption that mortar and PCM are the same temperature is only valid when using solid capsules with very high thermal

conductivity. The limited thermal conductivity in the PCM is well known, being around 0.2 W/m.K in paraffin and fatty acids and around 0.6 W/m.K in salts hydrate **[32-33]**

For non-local thermal equilibrium, there is a temperature difference between mortar and PCM phases in the porous medium. Therefore, a separate energy equation should be written for each phase.

For mortar phase, the energy equation can be written in the following form:

$$(1-\varepsilon)(\rho c)_B \frac{\partial T_B}{\partial t} = (1-\varepsilon).k_B \left(\frac{\partial^2 T_B}{\partial r^2} + \frac{1}{r}\frac{\partial T_B}{\partial r} + \frac{\partial^2 T_B}{\partial z^2} \right) + U.a.\left(T_{pcm} - T_B\right) \quad \textbf{(6)}$$

where ρ_B and c_B are, respectively the density and the specific heat capacity of the building material, k_B is the effective thermal conductivity of the building material, U is the heat transfer coefficient between the micro-encapsule of PCM and the cement mortar, ε is the volume percentage of the PCM in the mortar. The superficial capsule area per unit volume a is usually represented as a function of the diameter of the microcapsule d and ε as follows:

$$a = \frac{6.\varepsilon}{d} \quad \textbf{(7)}$$

The left hand side of **Eq.(6)** indicates the rate change of the mortar enthalpy in the VER. The first term on the right hand side represents the heat exchanged by conduction in the axial and radial directions in the VER. The second term describes the heat exchange by convection between the microencapsulated PCM and the mortar.

For microencapsulated PCM, the energy equation takes the form of

$$\varepsilon(\rho c)_{pcm} \frac{\partial T_{pcm}}{\partial t} = U.a.\left(T_B - T_{pcm}\right) - \varepsilon.\rho_{pcm} L_f \frac{\partial f}{\partial t} \quad \textbf{(8)}$$

where k_{PCM} is the thermal conductivity of the PCM, ρ_{PCM} its density and c_{PCM} its specific heat capacity and T_m is the melting temperature of the PCM. In **Eq.(8)**, the left hand side represents the rate of enthalpy change of the PCM within the control volume. The first term

on the right hand side indicates the heat conduction in the axial and radial directions in the control volume while the second term represents the convection heat transfer between the microencapsulated PCM and the mortar while the last term describes the evolution of the latent heat during the phase change of the PCM.

When the PCM is at solid or liquid state (i.e. $f = 1$ for fully liquid control volume and $f = 0$ for fully solid control volume), **Eq.(8)** can be written as:

$$\varepsilon(\rho c)_{pcm} \frac{\partial T_{pcm}}{\partial t} = U.a.(T_B - T_{pcm}) \quad \textbf{(9)}$$

During the phase transition (melting or freezing), the PCM temperature remains constant ($T_{pcm} = T_m$) and **Eq.(8)** can be written as:

$$\varepsilon.\rho_{pcm} L_f \frac{\partial f}{\partial t} = U.a.(T_B - T_m) \quad \textbf{(10)}$$

To take into account the air between the building material and the cover of the cell, we consider two different heat exchange coefficients $K_1$and K_2 (see **Fig.2**). So the boundaries conditions are:

- ***Building material***

$$\left(\frac{\partial T_B}{\partial r}\right)_{r=0} = 0 \quad \textbf{(11)}$$

$$-\lambda_B \left(\frac{\partial T_B}{\partial r}\right)_{r=R} = K_2 (T_B - T_p) \quad \textbf{(12)}$$

$$-\lambda_B \left(\frac{\partial T_B}{\partial z}\right)_{z=0} = K_2 (T_B - T_p) \quad \textbf{(13)}$$

$$-\lambda_B \left(\frac{\partial T_B}{\partial z} \right)_{z=Z} = K_1 \left(T_B - T_p \right) \quad \textbf{(14)}$$

At $t = 0$ the initial conditions are $T_B(r,z,0) = T_{PCM}(r,z,0) = T_0$ and $f(r,z,0) = 0$. This implies that the PCM is at the solid phase at $t = 0$ and T_0 is lower than the melting temperature of the PCM.

As the thermal conductivity of air is smaller than that of the metal of the cell, we suppose that all the energy is communicated to the plate by the lower boundary of the cell. Moreover, we suppose that all the parts of the cell are at the plate temperature T_P. So, Φ is the sum of the thermal fluxes through the walls of the metallic cell [**30-31**] **:**

$$\Phi = -\sum_i K_i \left(T_{B,i} - T_{plt} \right) \Delta S_i \quad \textbf{(15)}$$

where $K_i = K_1 \; or \; K_2$ is the heat transfer coefficient and ΔS_i is the area of the different boundaries of the cell.

In our simulations the endothermic phenomena (melting) are presented towards positive ordinates whereas the exothermic phenomena (freezing) towards negative ordinates. The differential equations (3, 5 and 6) subjected to the initial and boundary conditions (7, 8, 9 and 10) have been solved numerically by using the control volume finite difference method. The sample is subdivided into control volumes, where the grid points are placed at the geometric centers of these control volumes. The differential equations are integrated over each control volume and over the time step. The time derivatives have been approximated by using fully implicit time integration. The resulting discrete equations at each time step have been solved iteratively by using Tridiagonal Matrix Algorithm (TDMA).

4. Specific enthalpy and specific heat capacity of the sample

A principle motivation of using phase change materials is to profit from the latent heat or the specific enthalpy function during the phase change process. Due the heat transfer between the microencapsulated PCM and the building material, **Eq.(12)** can be used to calculate the specific enthalpy of the sample.

$$h_{sample} = \varepsilon . h_{pcm}^{tot} + (1-\varepsilon). h_B^{tot} \quad \textbf{(12)}$$

where

$$h_{pcm}^{tot} = \sum_{j=1}^{N} h_{\mathrm{pcm},j}(T_{\mathrm{pcm},j}) \quad \textbf{(13)}$$

and

$$h_B^{tot} = \sum_{j=1}^{N} h_{\mathrm{B},j}(T_{\mathrm{B},j}) \quad \textbf{(14)}$$

where N is the number of control volume in the sample.

In this work, the reference state for the specific enthalpy is chosen to be the liquid phase for PCM and the pressure is supposed to be constant, equal to 1 atm. The enthalpy of the pure PCM at solid state, the pure PCM at liquid state and the building material in each control volume can be calculated by the following expressions:

$$h_B(T_B) = \int_{T_i}^{T_B} c_B(T_B) dT_B \quad \textbf{(15)}$$

$$h_{pcm}(T_{pcm}) = L_F + \int_{T_i}^{T_{pcm}} c_{pcm}(T_{pcm}) dT_{pcm} \quad \textbf{(16)}$$

During the melting process, the specific enthalpy of the PCM can be estimated by using the following expression:

$$h_{pcm}(T_m) = f . h_{\mathrm{pcm},l}(T_m) + (1-f). h_{\mathrm{pcm},s}(T_m) \quad \textbf{(17)}$$

It is interesting to note that there is a discontinuity of the enthalpy function when the PCM temperature approaches that of the melting temperature T_m. This discontinuity can be expressed as:

$$\Delta h_{pcm} = \lim_{T_{pcm} \to T_m^+} h_{pcm} - \lim_{T_{pcm} \to T_m^-} h_{pcm} = h_{pcm}(T_m^+) - h_{pcm}(T_m^-) \neq 0 \quad \textbf{(18)}$$

where

$$h_{pcm}(T_m^+) = f.h_{\text{pcm},l}(T_m^+) + (1-f).h_{pcm,s}(T_m^+) \quad \textbf{(19)}$$

$$h_{pcm}(T_m^-) = f.h_{\text{pcm},l}(T_m^-) + (1-f).h_{pcm,s}(T_m^-) \quad \textbf{(20)}$$

From a mathematical point of view, **Eq.(17)** is non-differentiable at T_m and the apparent heat capacity $c_{p,app}$ of the pure PCM becomes infinite during the melting process.Certain users of the DSC device define an equivalent heat capacity by using the following expression:

$$c_{p,eq} = \frac{\Phi}{\text{m}.\beta} \quad \textbf{(21)}$$

where m is the mass of the sample.

5. Model validation

The validation of the present physical model is carried out on the basis of the experimental work mentioned in References**[11-12]** in which mortar with 20% of PCM is placed in a rectangular mould with the interior dimension of 25×25×4 cm^3 [**11-12**]. The PCM has a fusion temperature equal to +26 °C. The thermophysical properties of mortar and PCM are summarized in **Table 1-a** and **Table 1-b**. Each side of the rectangular wallboard is exposed to a linear time-dependent surface temperature from 11 to 40°C.

Fig.3 illustrates the temperature variation at the centre of the rectangular wallboard versus the specified linear temperature. It is found that the temperature at the middle of the sample is not linear and has an inflection point, which clearly indicates a latent thermal storage process during melting and freezing of the PCM inside the mortar. It is also noted that the phase change process commences at the fusion temperature of the PCM.

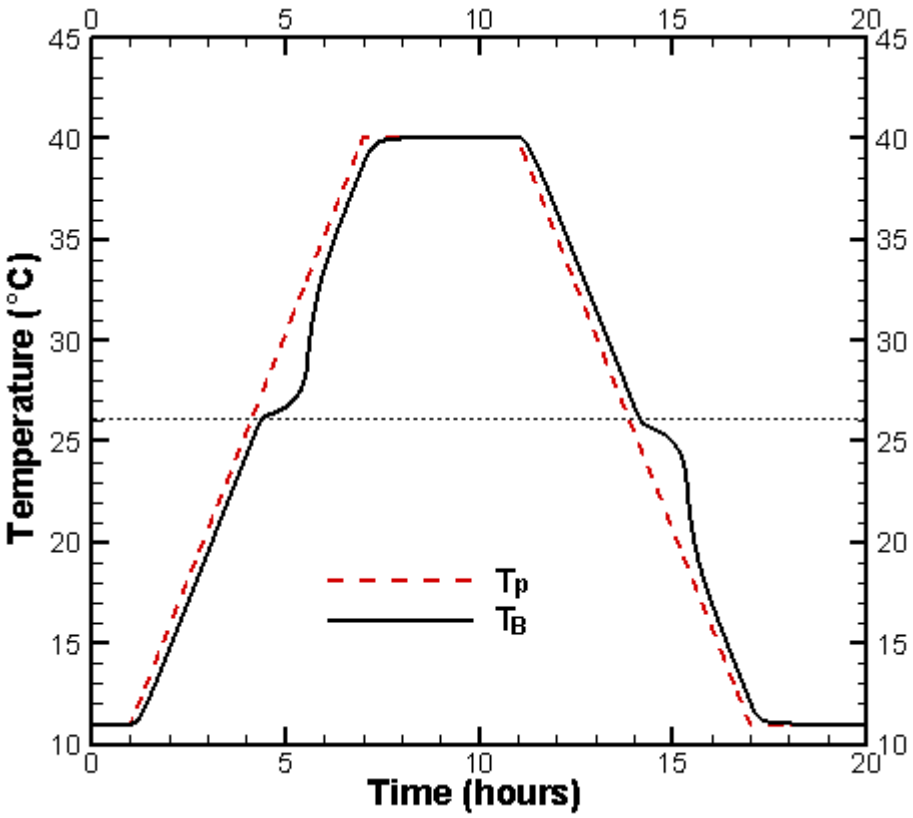

Fig.3: Mortar temperature variation with time during melting and solidification processes [10,13].

Fig.4 presents the experimental and numerical heat fluxes on the left side of the rectangular wallboard. It can be seen from this figure that there is reasonable consistency between the current physical model and the experimental results during the melting process. However, the difference between the experimental heat flux and the numerical heat flux can be assigned to the following factors. In the physical model, PCM is assumed to melt at a constant temperature. These discrepancies can also be explained by the presence of the foreign substances in the PCM under study.

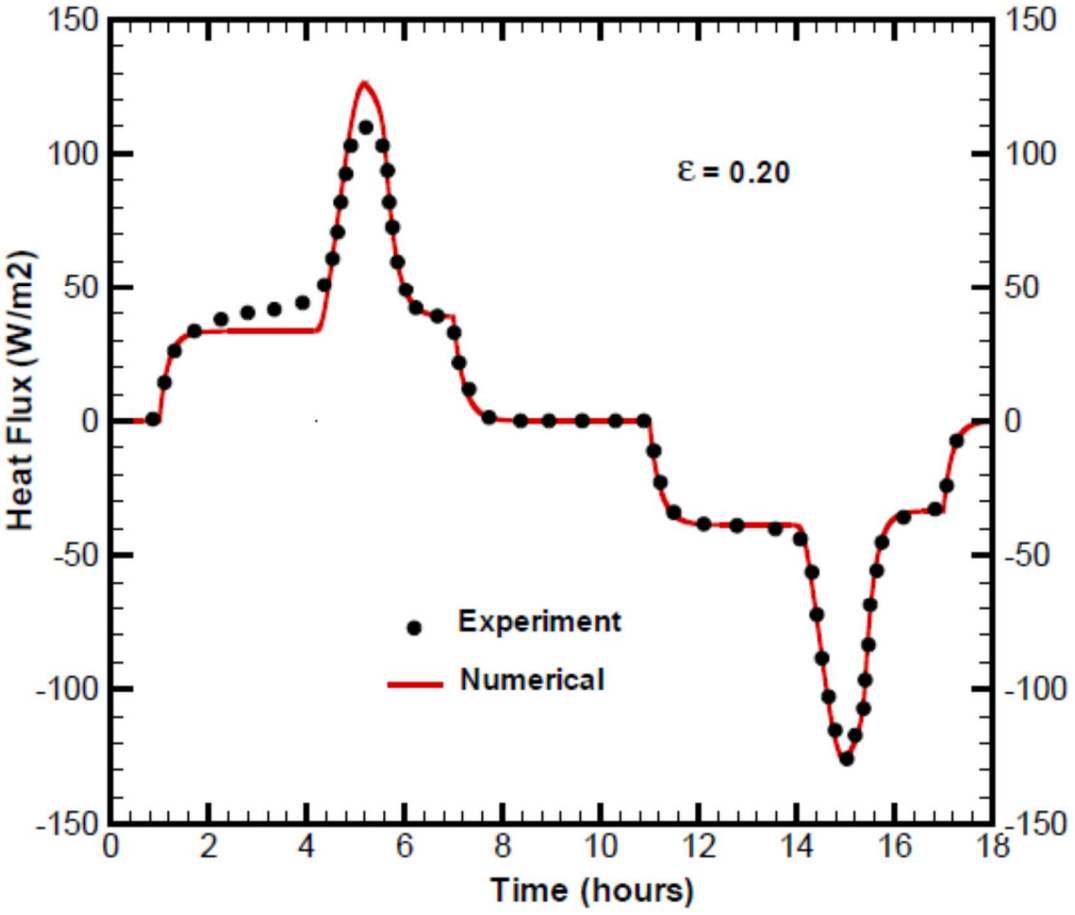

Fig.4: Heat flux through heating and cooling cycles at the front face of the mortar [10, 13].

6. Results and discussion

The physical model described in section 3 is used to determine the DSC curve (see **Fig.5**), the global liquid fraction (see**Fig.5**) and the temperature distribution (see**Fig.6**) inside the mortar containing the microencapsulated PCM,

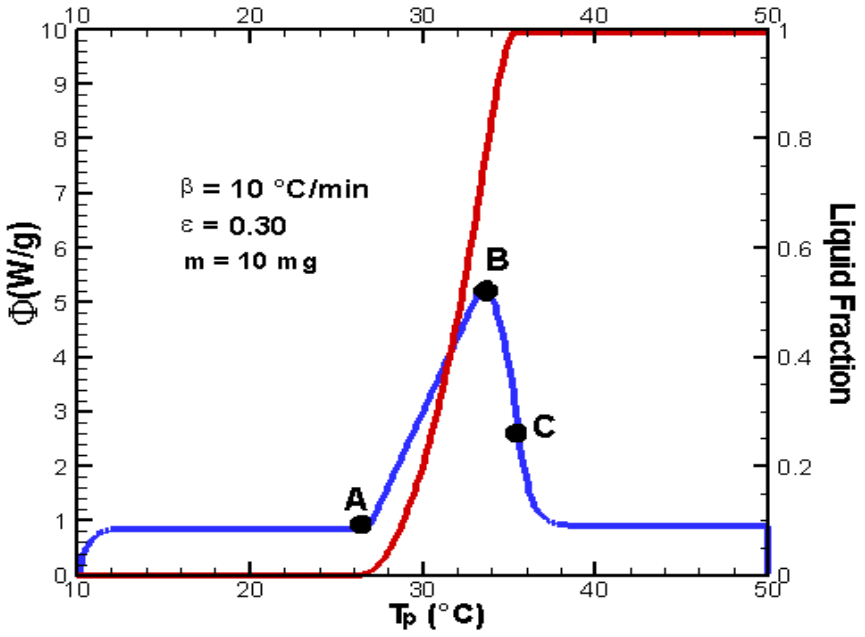

Fig.5: Numerical DSC curve and global liquid fraction of the PCM versus the plate temperature

The melting process of the microencapsulated PCM inside the sample leads to an endothermic DSC signal as presented in**Fig.5**. One can remark that the DSC signal exhibits a certain width during the melting process of the microencapsulated PCM. This does not signify that the melting process takes place over a temperature range but only it requires a long time to progress through the entire sample. The variation of the global liquid fraction versus the plate temperature T_p inside the sample (see **Fig.5**) can be used to explain the shape of the DSC curve and to determine the beginning (**A**)and the end point (**C**) of the melting process. The DSC curve can also be characterized by the point (**B**) which is corresponding to the instant when the heat flux recorded by the DSC is maximum.

Most users of the power compensation DSC device assume that the temperature of the sample inside the DSC cell is uniform. This suggests that the plate temperature T_p is the characteristic temperature of the sample. Theoretically, when a mortar integrating a microencapsulated PCM, is subjected to continuous heating, temperature gradients inside the mortar arise during the phase change process. To illustrate this effect, we have presented on **Fig.6** the temperature variation of both microencapsulated PCM and building material at various positions inside the sample versus the plate temperature T_p. We remark that the melting of the PCM inside the sample at different positions occurs at a constant temperature $T_{PCM} = T_m$. The building material temperature T_B exhibits a deviation during the heating cycle due to the melting process of the PCM inside the mortar and the plate temperature T_P increases continuously

without being affected by the melting process inside the sample (see **Fig.6**). It can be mentioned that even with a small sample size (m = 10 mg), there is a considerable temperature gradient inside the mortar during the fusion process, whereas during the sensible storage (i.e. outside the phase change transition) the thermal gradients inside the building material are relatively negligible. One can conclude that the representative temperature of the mortar cannot be attributed to the plate temperature during the phase change transition process of the PCM.

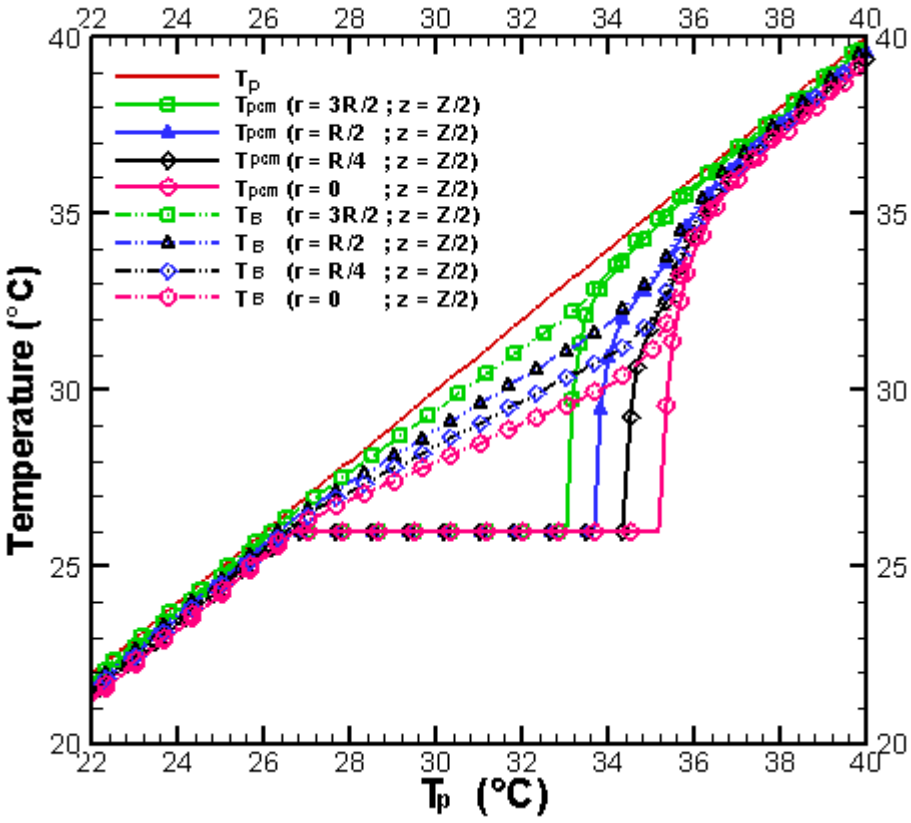

Fig.6: Variation of the sample temperature versus the plate temperature at various positions inside the sample.

We can also note that the resulting specific enthalpy, apparent specific heat capacity and equivalent specific heat capacity values of the sample calculated according to the plate temperature T_P are systematically enlarged the temperature range of the melting process of the PCM (see **Figs 7-a, 7-b and 7-c**). We remark that both functions (the specific enthalpy and the equivalent specific heat capacity of the sample) have no discontinuity during the phase

change process, whereas the apparent specific heat capacity of the sample shows a discontinuity towards the end of melting process.

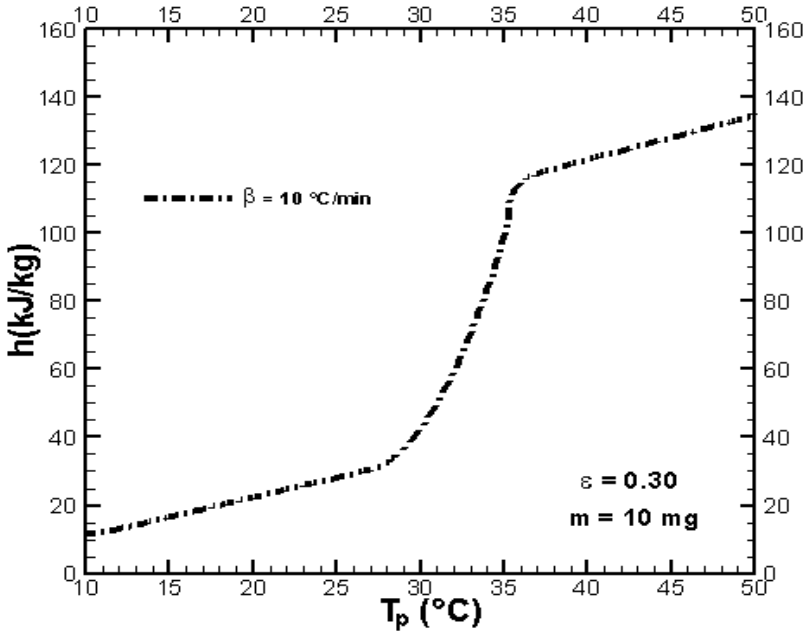

Fig.7-a: Specific enthalpy of the sample versus the plate temperature

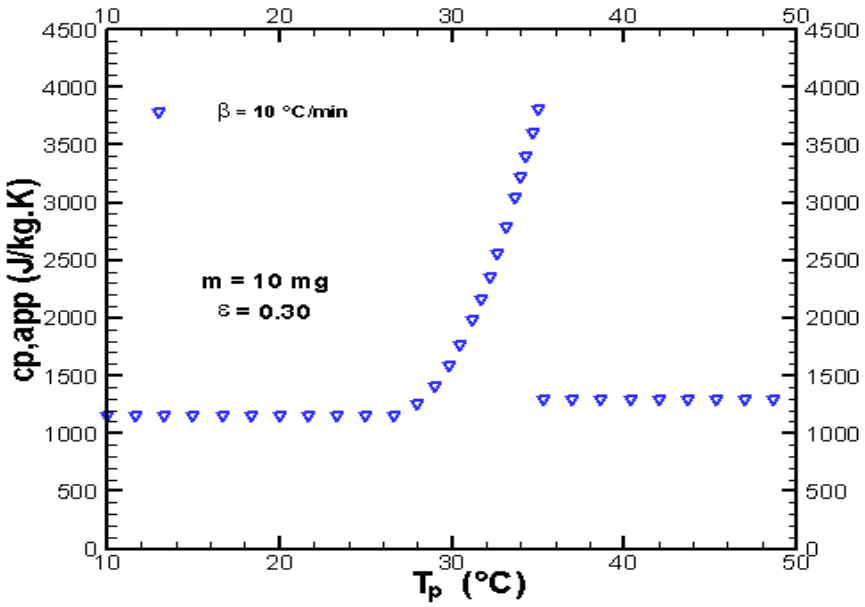

Fig.7-b: Apparent heat capacity of the sample versus the plate temperature

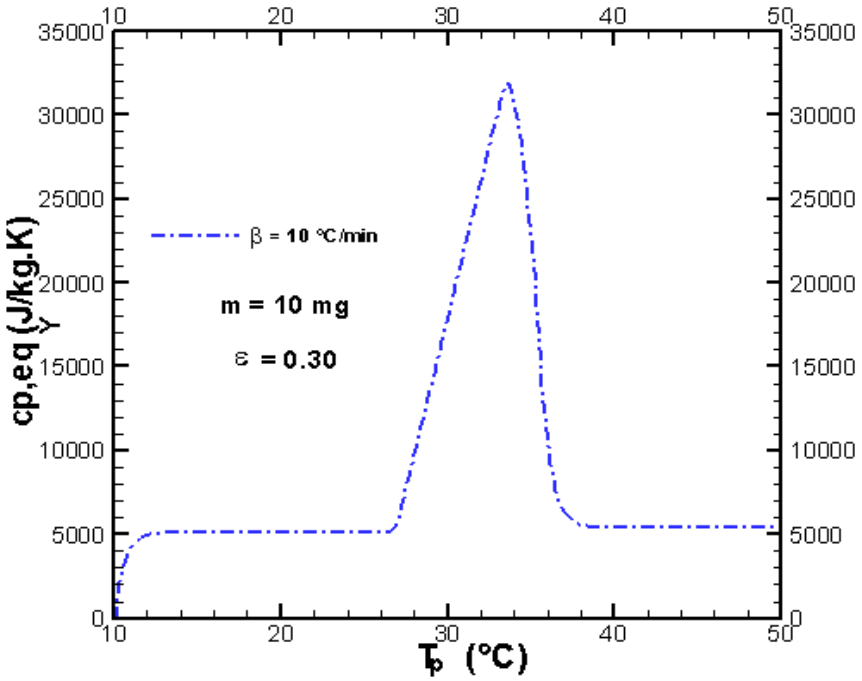

Fig.7-c: Equivalent heat capacity of the sample versus the plate temperature

Theoretically, the specific enthalpy and the apparent heat capacity functions present a discontinuity during the melting process of the pure PCM. We consider that when the DSC apparatus is chosen to determine the specific enthalpy and the apparent heat capacity of the pure PCM, it is more logical to present and determine these functions according to the representative temperature of the sample (for example the PCM temperature at the center of the sample) and not according to the plate temperature as one can be seen in **Figs 8-a and 8-b**. The judicious choice of the representative temperature of the sample permits to describe faithfully the variation of the specific enthalpy and the apparent specific heat capacity of the sample during the melting process. Unfortunately this temperature is inaccessible from DSC device. Consequently, the most users of the DSC device determine the specific enthalpy, the equivalent heat capacity and the apparent heat capacity according to the plate temperature. As a result, the measured enthalpy and the heat capacity of the PCM during the melting process can be overestimated or underestimated during the continuous heating and important inaccuracies can be engendered during these tests.

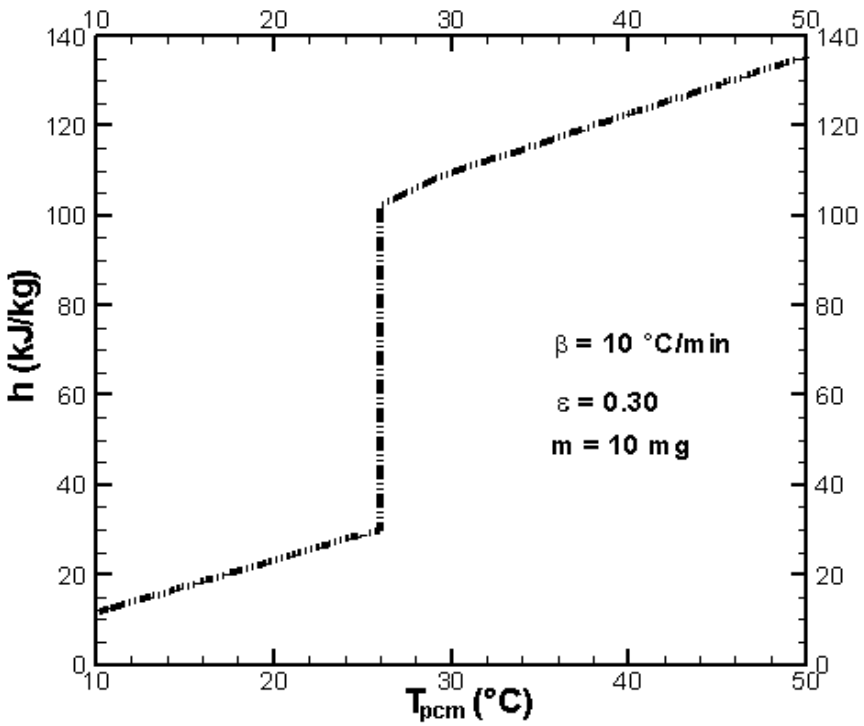

Fig.8-a: Specific enthalpy of the sample versus the PCM temperature

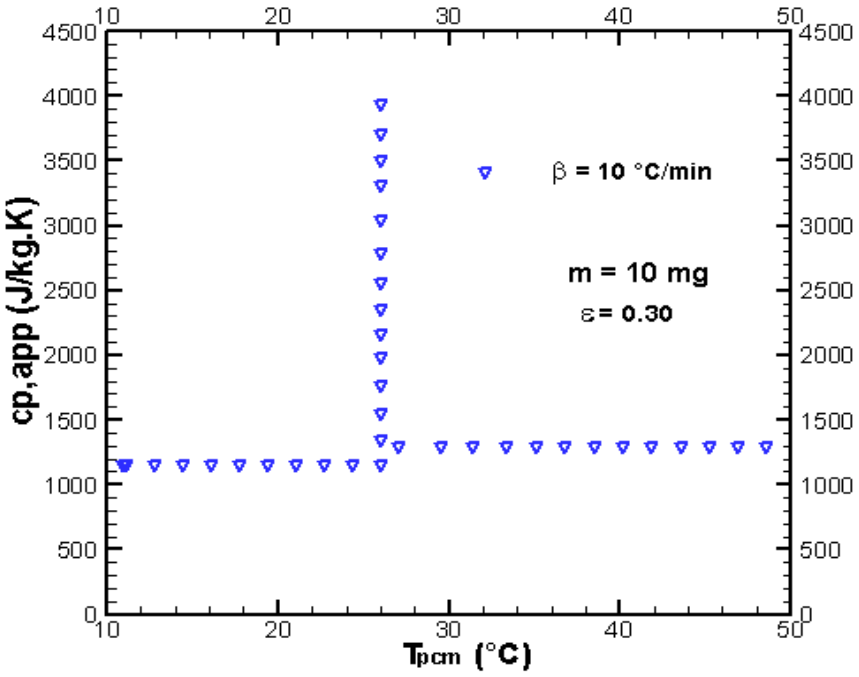

Fig.8-b: Apparent heat capacity of the sample versus the PCM temperature

6.1 Effect of the heating rate β

Fig.9-a and **Fig.9-b** present the numerical DSC curves for different heating rates. Even if the melting of the PCM occurs at constant temperature ($T = T_m$), the numerical DSC thermograms are highly dependent on the heating rate and the peak maximum temperature (which is corresponding to the point B) increases with increasing the heat rate (see **Figs 9-a and 9-b**).The melting temperature range becomes larger and it turns to greater temperature with increasing heating rate (see **Fig.9-a**).We can also observe that the increase in the heating rate reduce the duration of the melting process of the PCM inside the sample (see**Fig.9-b**). Important temperature gradient can be observed inside the sample during the melting process of the PCM due to the increase in the heating rate (see **Fig.10)**.

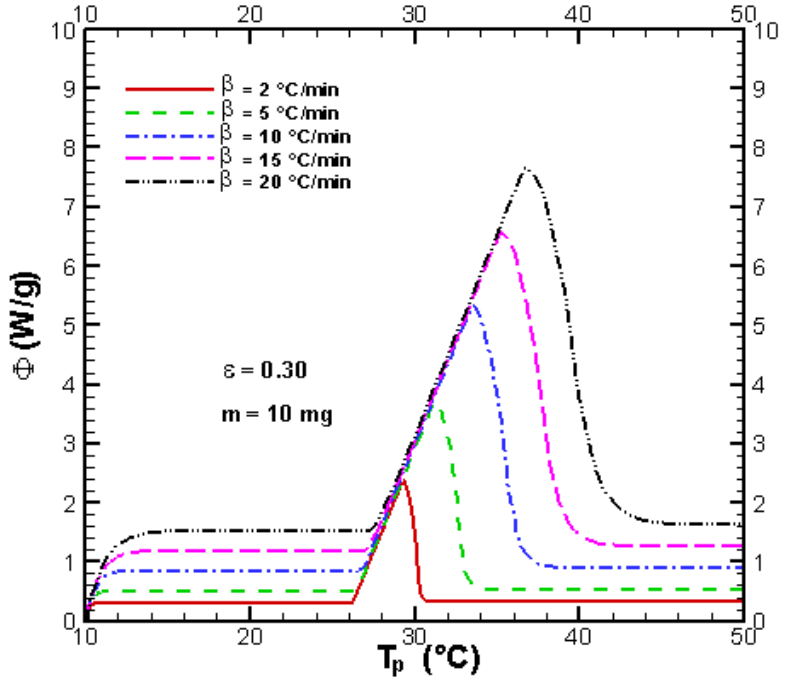

Fig.9-a: DSC curve versus the plate temperature for various heating rates

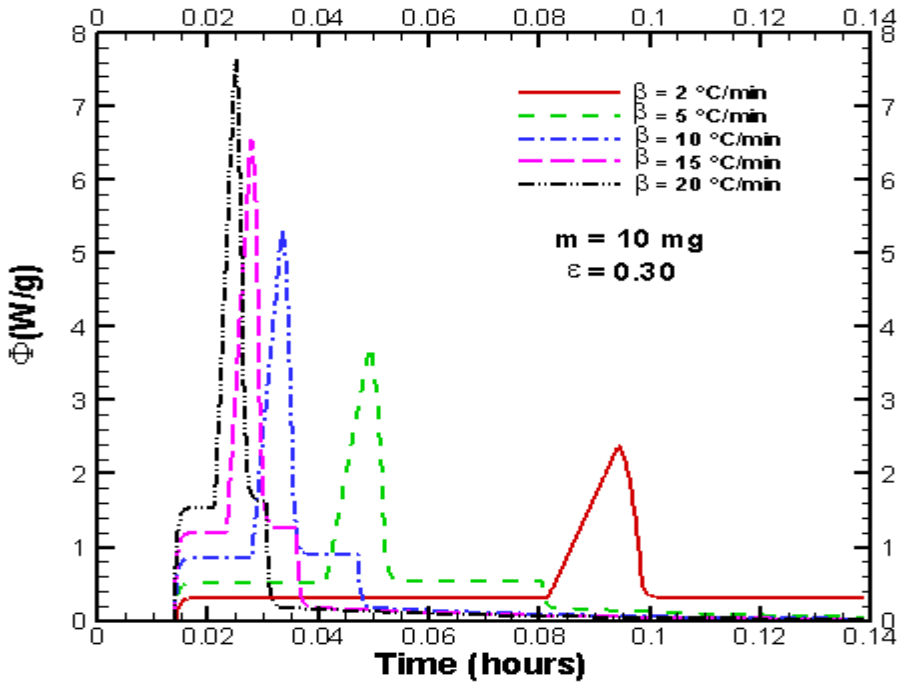

Fig.9-b: DSC curve versus time for various heating rates

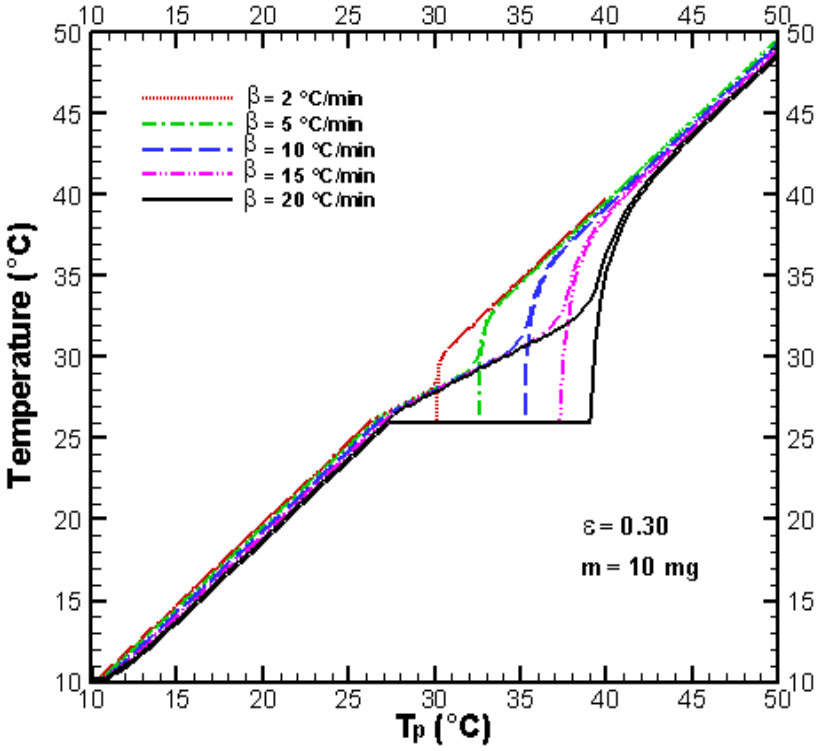

Fig.10: Temperatures of the building material and the microencapsulated PCM at the center of the sample versus T_p for various heating rates

We can note that the specific enthalpy, the apparent heat capacity and the equivalent heat capacity functions are systematically pushed to higher temperatures by increasing the heating rate (see **Figs 11-a, 11-b and 11-c**). This result can be attributed to the increase in the thermal gradient inside the sample as a result of the rise in the heating rate. Unfortunately most common users of the power compensation DSC device employ the plate temperature to determine the specific enthalpy, the apparent heat capacity and the equivalent heat capacity of the PCM without taking into account the effect of the heating rate and the thermal gradient inside the sample.

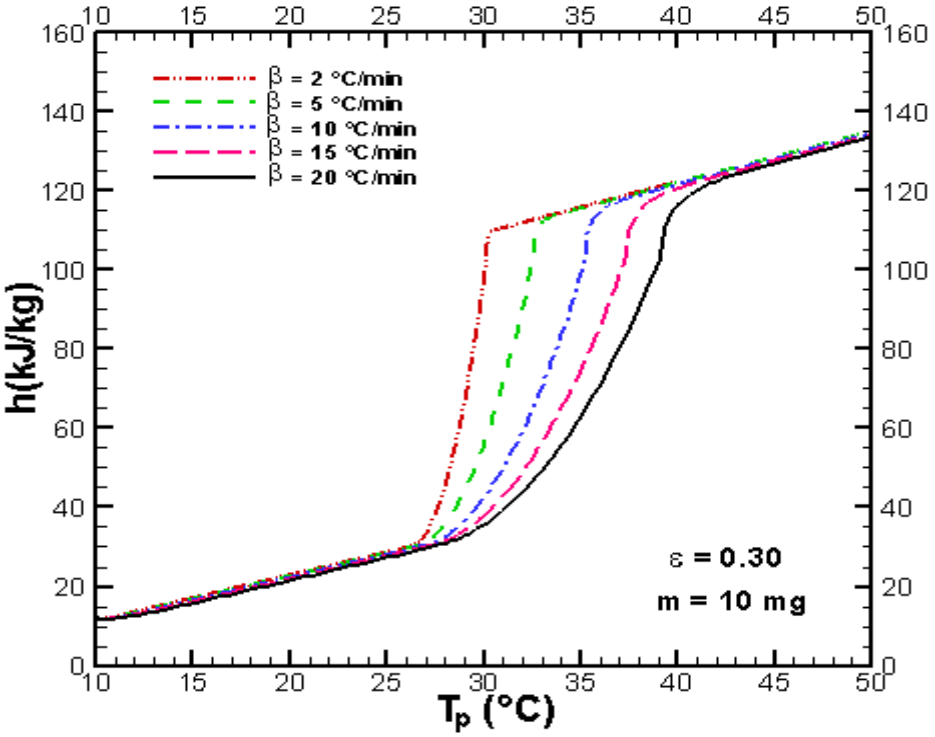

Fig.11-a: Specific enthalpy of the sample versus T_p for various heating rates

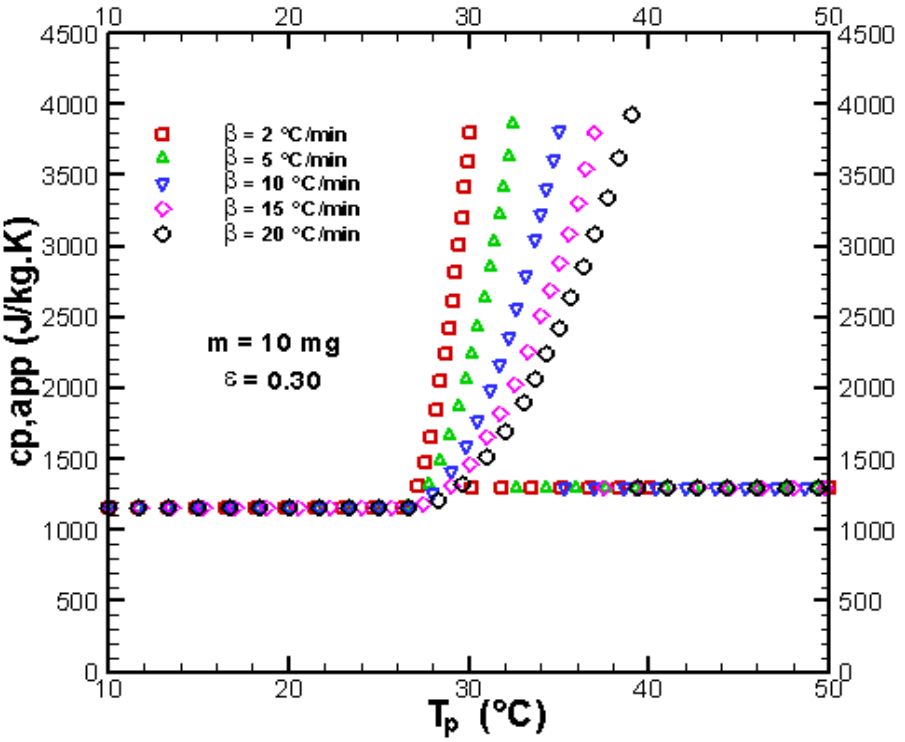

Fig.11-b: Apparent heat capacity of the sample versus T_p for various heating rates

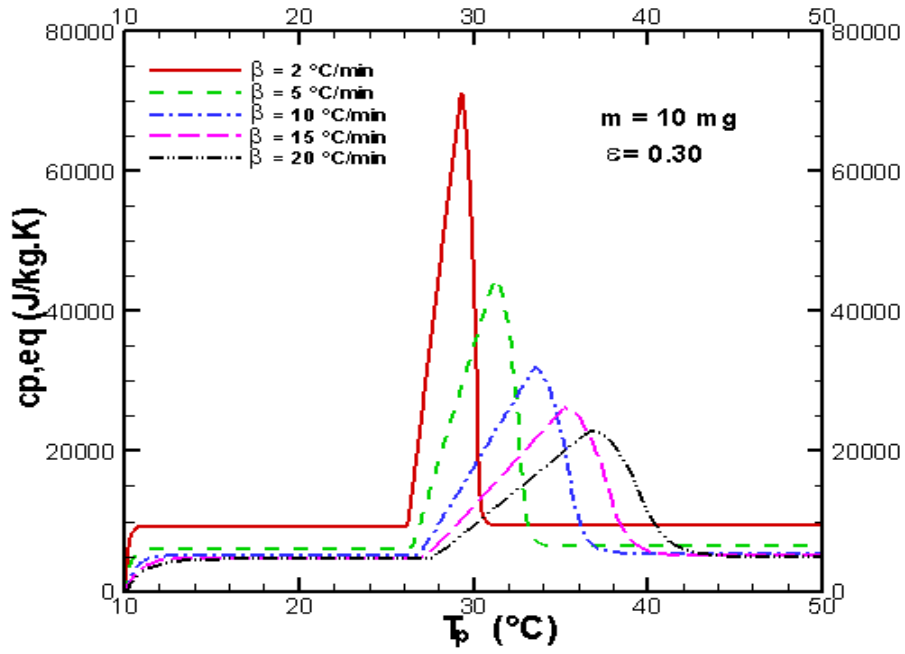

Fig.11-c: Equivalent heat capacity of the sample versus T_p for various heating rates

The examination of **Fig.9-a** revealed that for various heating rates all points **C** (which is corresponding to the end point of the melting inside the sample) form a line L_A, which cuts the axis of abscissas at the melting temperature of the PCM (see **Fig.12**). We can also observe that for different heating rates, the points **B** are aligned and formed the straight line L_B which cuts the axis of abscissas at the melting temperature of the PCM. One can remark that the intersection of the two lines (L_A and L_B) given on the axis of abscissa coincides perfectly with the melting temperature of the PCM and indicates the limit of the thermogram when $\beta \to 0$. We can also note that the difference between the peak temperature (point **B**) and the end point of the melting process (point **C**) becomes important by increasing the heating rate. These results can be explained by the fact that when the heating rate is close to zero, the temperature gradient inside the test sample become negligible and the end point of melting process (point **C**) corresponds practically to the maximum peak (point **B**). As a result the heating rate must be sufficiently reduced to guarantee thermodynamic equilibrium inside the test sample. As one can be seen in **Fig.11-a,** the specific enthalpy function should converge towards the correct value for low heating rate.

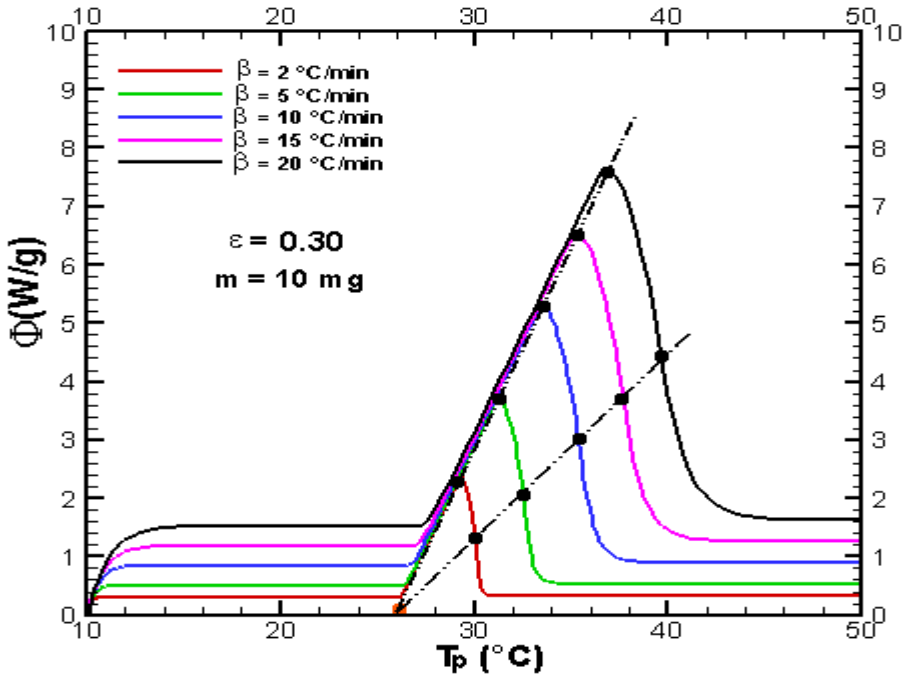

Fig.12: Heat flow rate versus T_p for various heating rates

6.2 Effect of the sample mass

The calculated DSC thermogram for various mass of the sample at constant heating rate is presented on **Fig.13**. As can be seen in **Fig.13** the width of the DSC curve and the maximum peak corresponding to the point **B** decrease with increasing the mass of the sample. It is easy to see in **Fig.14,** that the temperature gradient inside the test sample increases as the sample mass increases from 6 mg to 14 mg. The specific enthalpy, the apparent heat capacity and the equivalent heat capacity the sample are also affected by the variation of the mass of the sample between 6 mg and 14 mg (see **Figs 15-a, 15-b and 15-c**). One can conclude that the users of the DSC instrument must pay attention to the interpretation and the reliability of the obtained measurements when varying the mass of the sample.

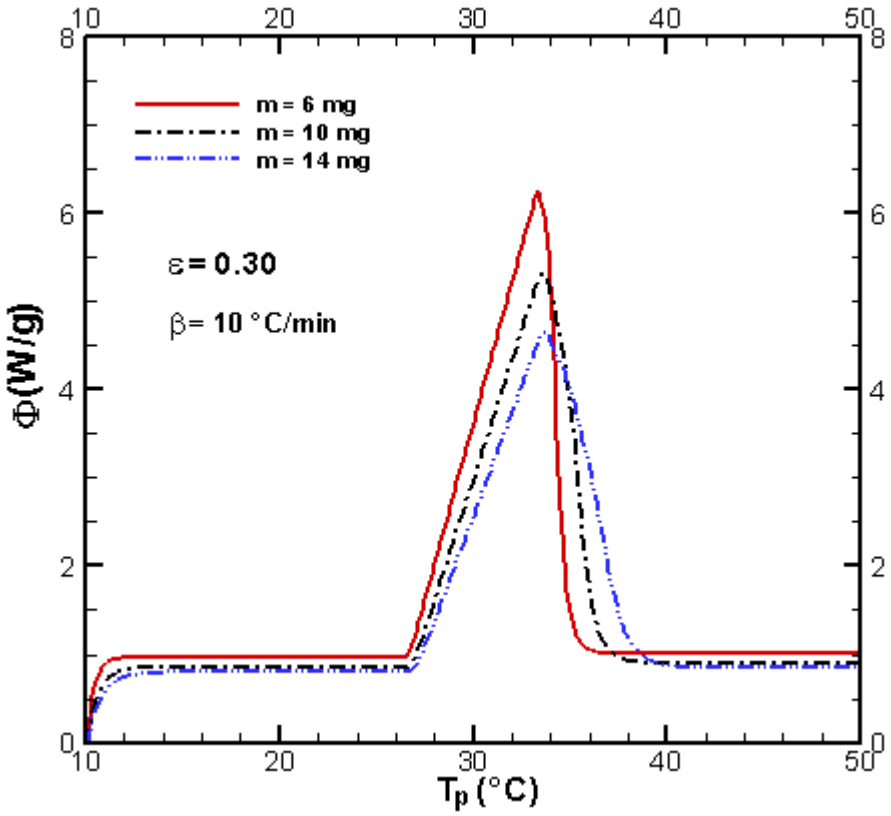

Fig.13: Heat flow rate versus T_p for various samples mass

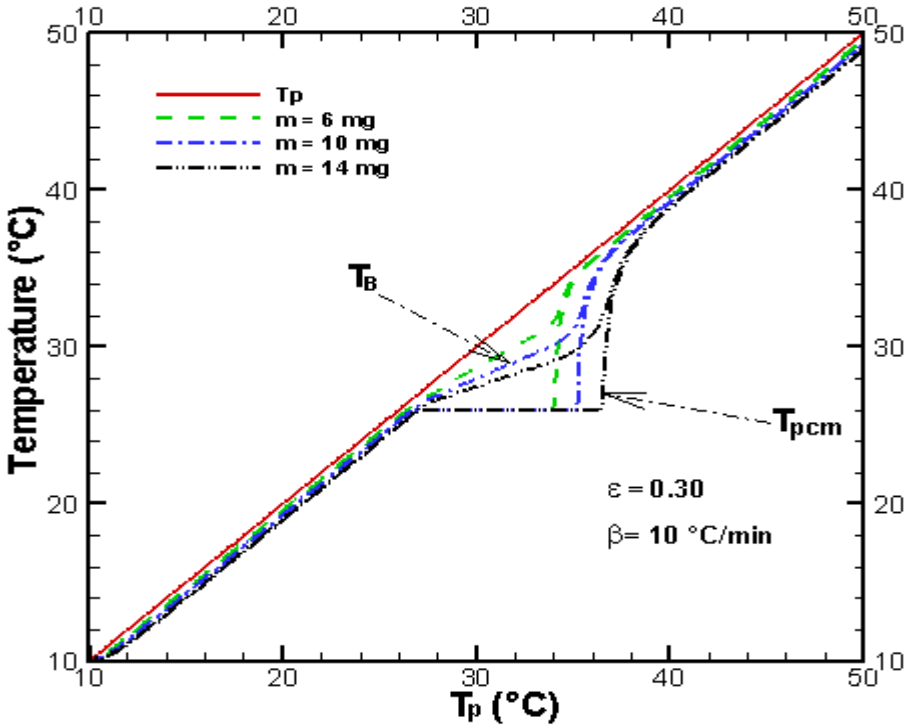

Fig.14: Temperatures of the building material and the microencapsulated PCM at the center of the sample versus T_p for various samples mass

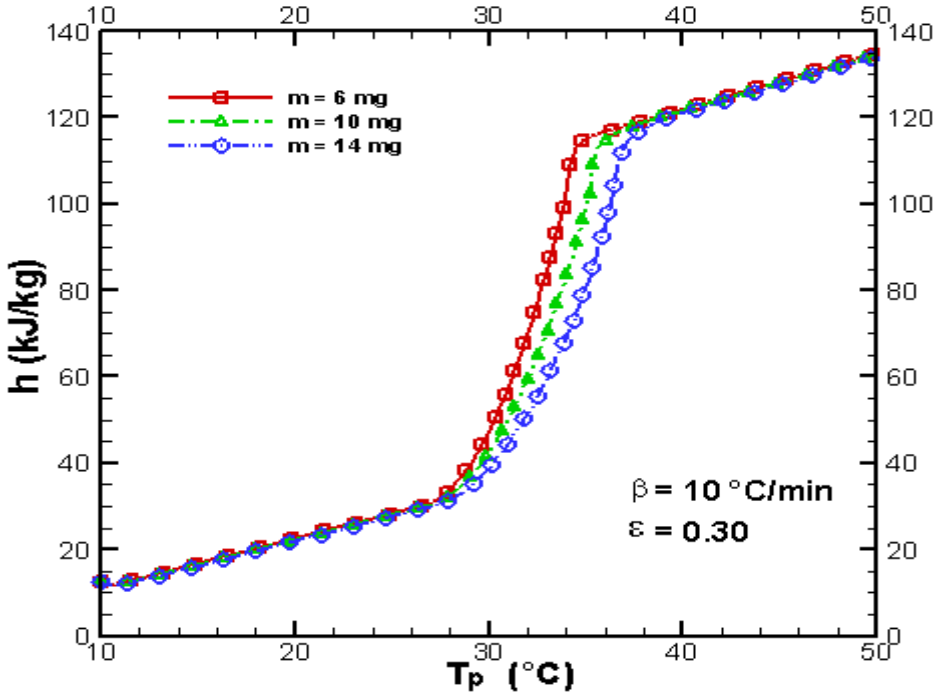

Fig.15-a: Specific enthalpy versus T_p for various samples mass

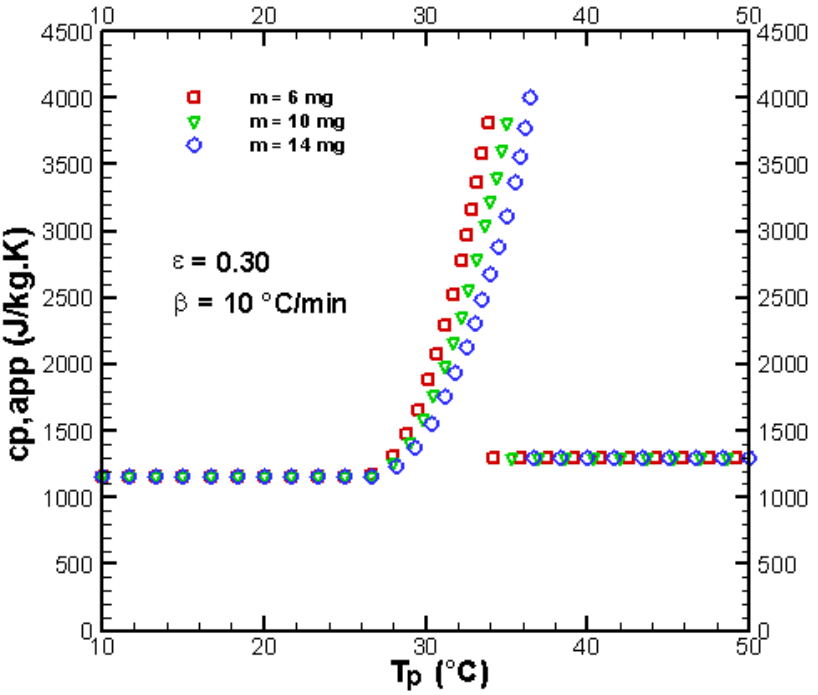

Fig.15-b: Apparent heat capacity versus T_p for various samples mass

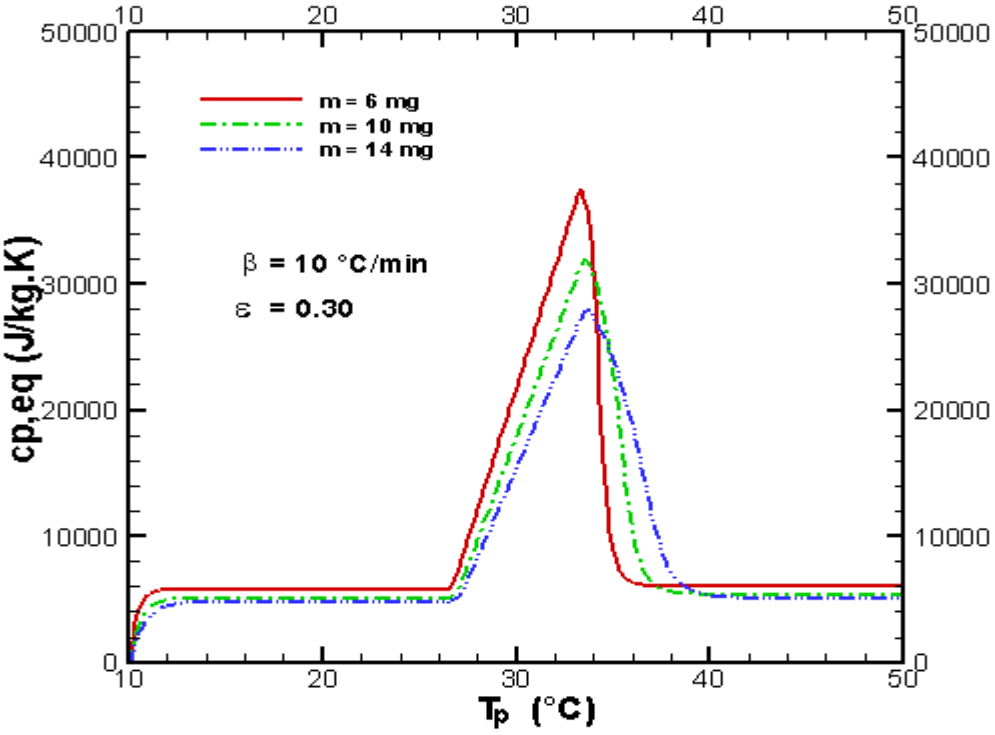

Fig.15-c: Equivalent heat capacity versus T_p for various samples mass

6.3 Effect of the volume fraction ε of the PCM in the building material

The numerical heat flow rate versus the plate temperature for different values of ε is showed on **Fig.16.** As can be seen the kinetics and the duration of the melting process of the PCM inside the test sample depends on ε . As the rise in the volume fraction of the microencapsulated PCM in the sample increases the time required for the melting process, the peak temperatures range becomes broader and its shifts to greater temperatures with increasing ε .We can conclude that the increase in the volume fraction of the PCM inside the sample produces temperature gradients inside the sample (see **Fig.17**). Consequently, the specific enthalpy, the apparent heat capacity and the equivalent heat capacity the sample are also impacted by the variation of the volume fraction of the PCM inside the sample (see **Figs 18-a, 18-b and 18-c**).

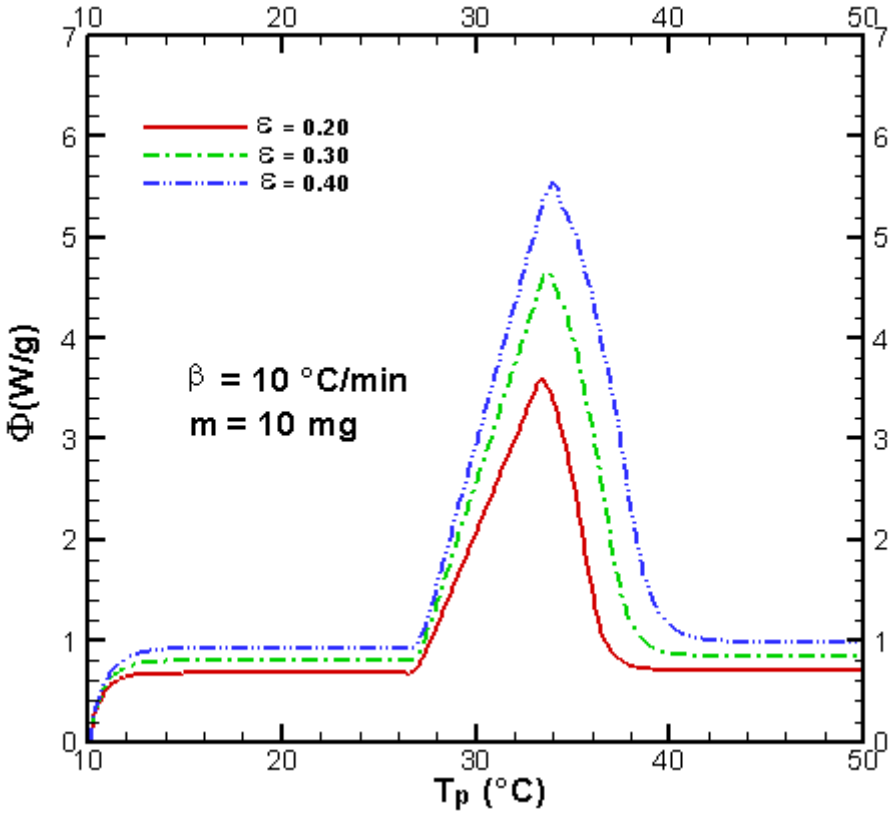

Fig.16: Heat flow rate versus T_p for various ε

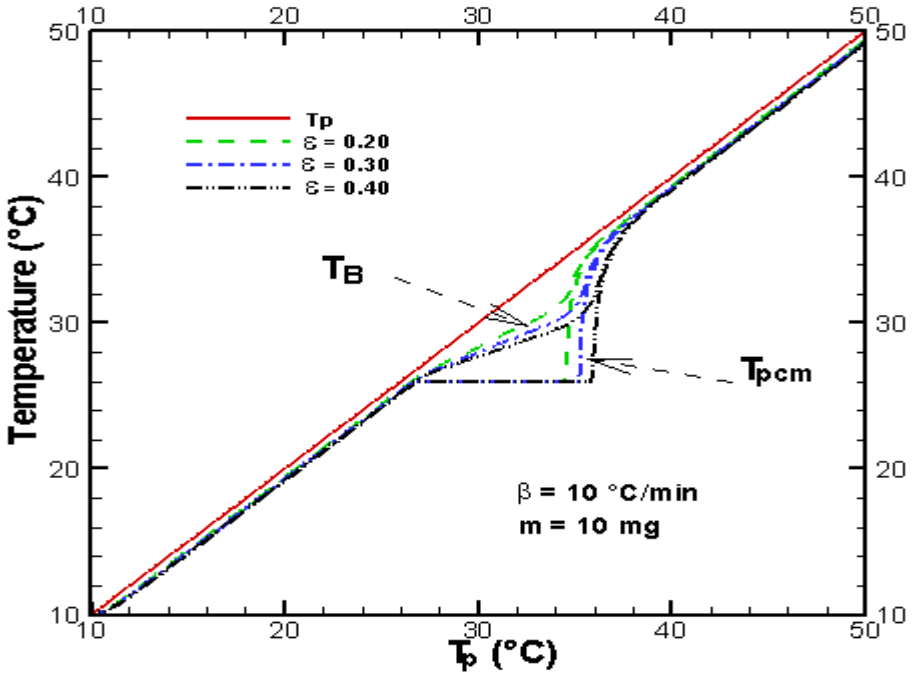

Fig.17: Temperatures of the building material and the microencapsulated PCM at the center of the sample versus T_p for various ε

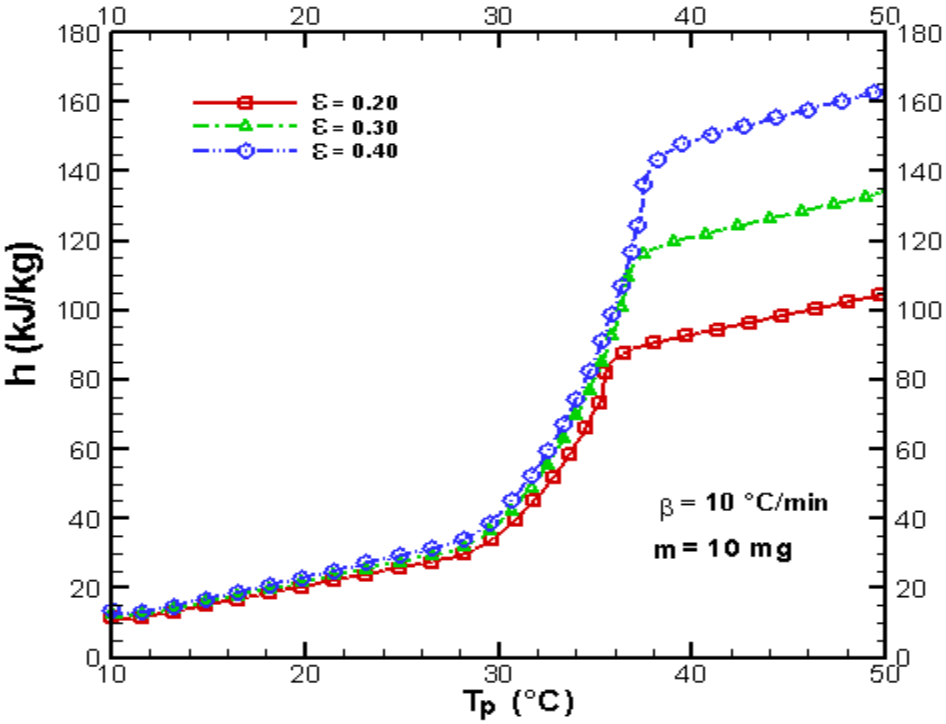

Fig.18-a: Specific enthalpy versus T_p for various ε

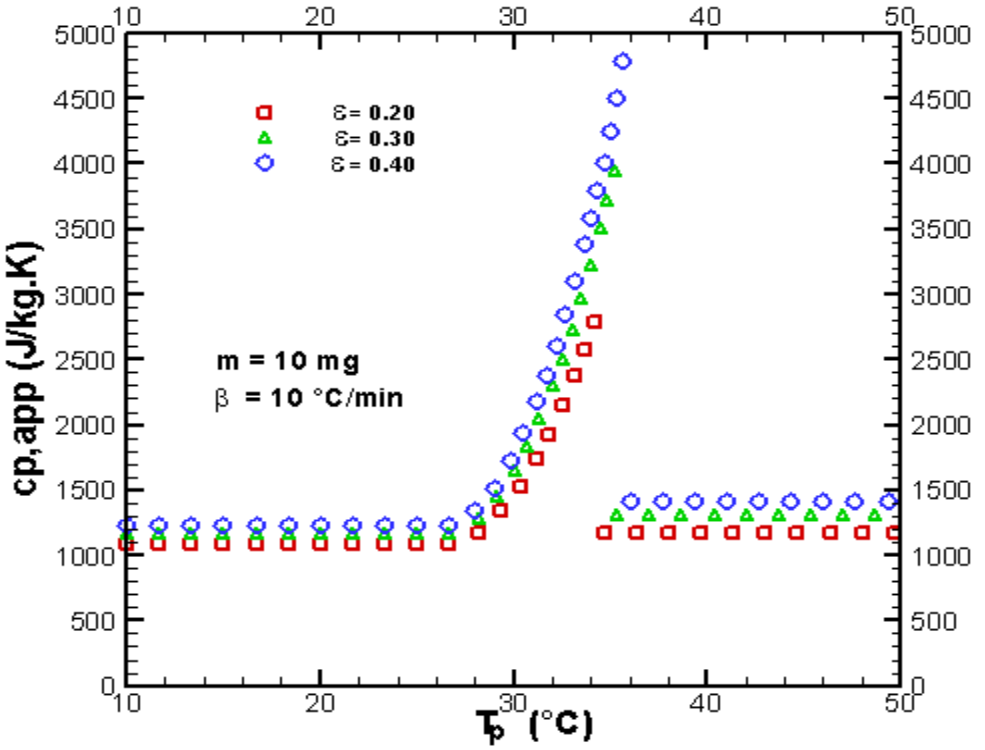

Fig.18-b: Apparent heat capacity versus T_p for various ε

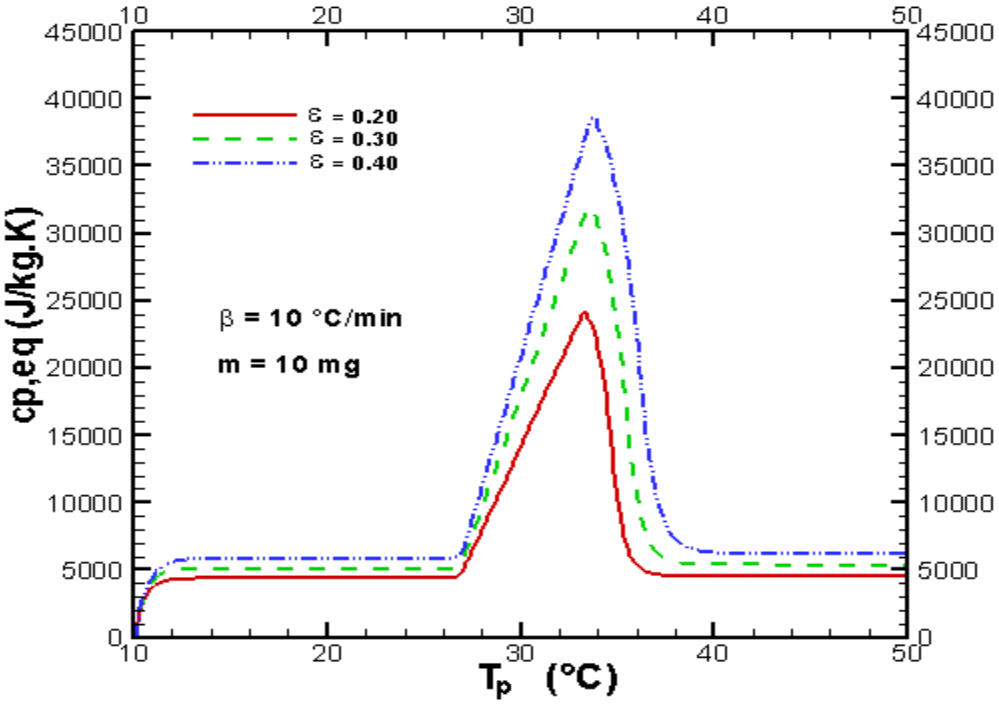

Fig.18-c: Equivalent heat capacity versus T_p for various ε

6.4 Hysteresis phenomenon

The hysteresis phenomenon is generally characterized by a total shifting of the enthalpy function during the solidification process of the PCM with respect to the same function during the melting process. A number of researchers comprehend hysteresis as property of the phase change material only **[34-36].** There are a various phenomena associated with the thermophysical properties of the material under study which can engender the hysteresis phenomenon. The most common one is supercooling [**34**]. Supercooling is the phenomenon that the PCM liquid does not crystallize, although its temperature is lower than the freezing point [**37-38**]. Another possible cause of the real hysteresis is when the latent heat is released too slowly during the freezing process because diffusion processes are necessary to homogenize the sample **[34]**. In our work the melting and the freezing processes are supposed to take place at the same temperature T_m, consequently the effect of the supercooling phenomenon is neglected.

To verify if the hysteresis phenomenon is present or not in our case, DSC curves in heating and cooling modes with the same rate are presented on **Fig.19**. One can see the usual shifting of the DSC thermograms towards the right (heating mode) and the left (cooling mode) respectively due to the impact of the heating/cooling rate on the thermal gradients inside the sample (see **Figs 20-a** and **20-b**). We notice that the specific enthalpy function of the sample is shifted towards the right (heating mode) and the left (cooling mode) respectively (see **Fig.21**). As a result, the hysteresis phenomenon is present in our case and it is amplified by increasing the rate of heating and cooling modes. The same effect is observed when varying the mass of the sample (see **Fig.22**). According to Mehling and Cabeza **[34],** the hysteresis phenomenon observed in our case is called apparent hysteresis phenomenon since it is only caused by the measurement conditions (i.e. thermal gradients inside the sample). It is important to remind that when the specific enthalpy of the sample is presented as a function of the representative temperature of the sample and not versus the plate temperature T_p the so-called apparent hysteresis phenomenon disappears (see **Fig.8-a**).

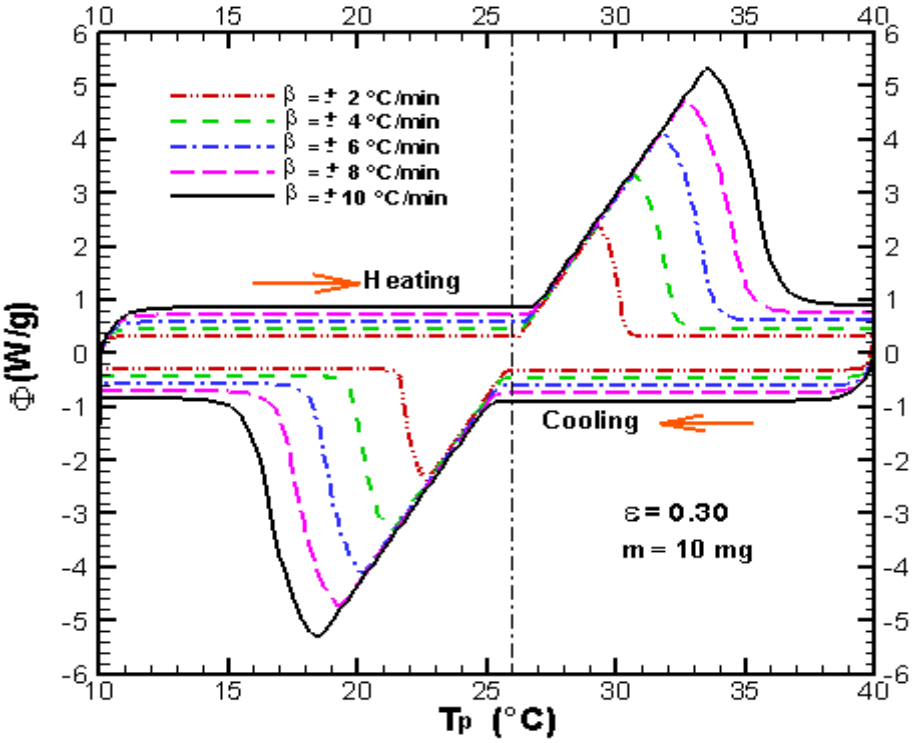

Fig.19: DCS curves in heating and cooling modes versus $T_p$for various rates

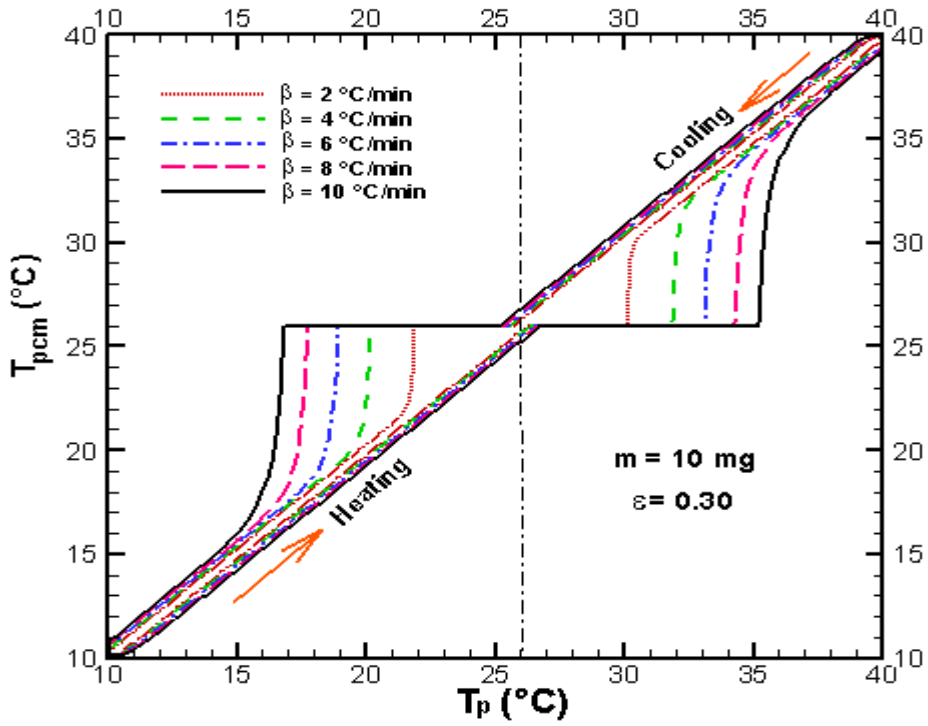

Fig.20-a: Microencapsulated PCM temperatures at the center of the sample in heating and cooling modes versus $T_p$for various rates

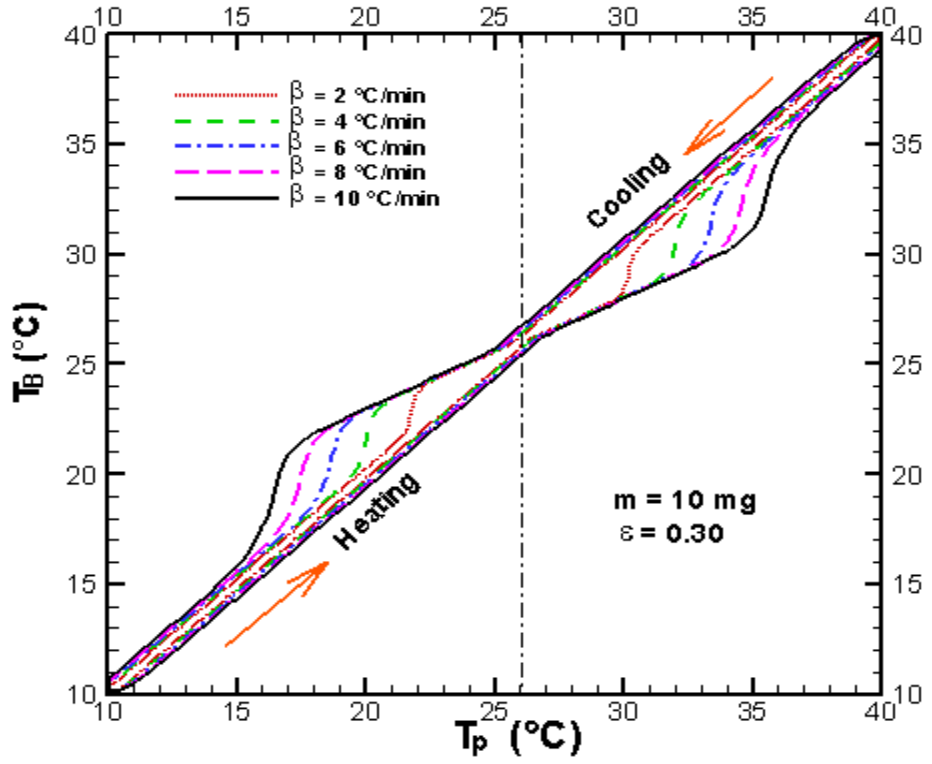

Fig.20-b: Building material temperatures at the center of the sample in heating and cooling modes versus $T_p$for various rates

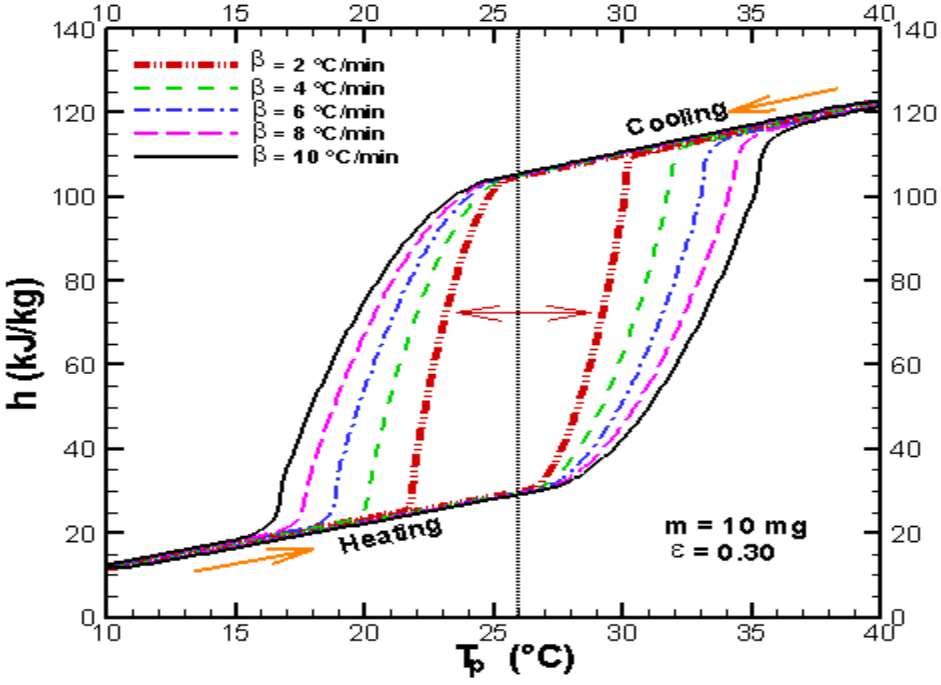

Fig.21: Specific enthalpy of the sample in heating and cooling modes versus $T_p$for various rates.

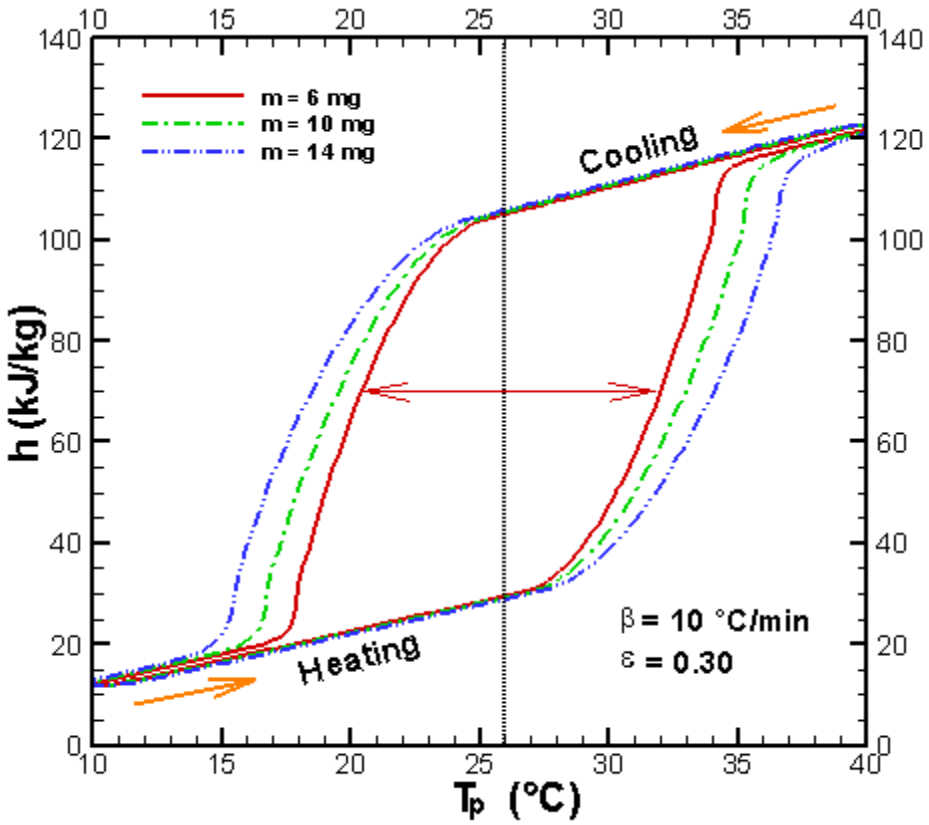

Fig.22: Specific enthalpy of the sample in heating and cooling modes versus $T_p$for various mass of the sample.

7. Conclusion

In this work, a physical model was performed to study the heat transfer inside a building material containing microencapsulated PCM in DSC cells. The general expressions of the specific enthalpy, the apparent heat capacity and the equivalent heat capacity are exposed. The effect of various parameters like the heating/cooling rate, the volume fraction of the PCM and the sample masse on the thermal behavior of these materials is investigated and discussed. Despite the small dimensions of the DSC cell, important thermal gradient has been observed during the phase change process of the PCM, responsible for the shape of the thermograms. These gradients become more and more important as the heating/cooling rate, the sample

mass changes and the volume fraction of the PCM increases. As a result, the values of the specific enthalpy, the apparent heat capacity and the equivalent heat capacity can be overestimated during the continuous heating or cooling processes. Due to these gradients, a significant inaccuracies can be generated and apparent hysteresis phenomenon can be observed during the heating or the cooling process. It is also demonstrated that the judicious choice of the representative temperature of the sample can reduce these inaccuracies. To ensure the thermodynamic equilibrium inside the composite material containing PCM, the heating/cooling rate and the sample mass should to be sufficiently reduced. Nevertheless, small sample mass refutes the necessity of having representative sample, and slow heating/cooling rate will lead to a low signal to noise ratio.

References

[1] L.Olivieri, J.A. Tenorio, D.Revuelta, L. Navarro, L. F. Cabeza, Developing a PCM-enhanced mortar for thermally active precast walls, Constr. Build. Mater. 181 (2018) 638-649.

[2] K. Biswas, J. Lu, P. Soroushian, S. Shrestha, Combined experimental and numerical evaluation of a prototype nano-PCM enhanced wallboard, Appl. Energy 131 (2014) 517-529.

[3] S. Ramakrishnan, X. Wang, J. Sanjayan, J. Wilson,Thermal performance assessment of phase change material integrated cementitious composites in buildings: Experimental and numerical approach, Appl. Energy 207 (2017) 654-664

[4] L. F. Cabeza, A. Castell, C. Barreneche, A. de Gracia, A.I. Fernandez, Materials used as PCM in thermal energy storage in buildings: A review, Renew. Sustain. Energy Rev. 15 (2011) 1675-1695.

[5] M. Bahrar, Z. I. Djamai, M. EL. Mankibi, A. Si Larbi, M. Salvia, Numerical and experimental study on the use of microencapsulated phase change materials (PCMs) in textile reinforced concrete panels for energy storage, Sustain. Cities Society 41 (2018) 455-468.

[6] L.F. Cabeza, C. Castellón, M. Nogués, M. Medrano, R. Leppers, O. Zubillaga, Use of microencapsulated PCM in concrete walls for energy savings, Energy Build. 39 (2007)113–119.

[7] Y. Konuklu, M. Ostry, H.O. Paksoy, P. Charvat, Review on using microencapsulated phase change materials (PCM) in building applications, Energy Build. 106 (2015) 134-155.

[8] M. Hunger, A.G. Entrop, I. Mandilaras, H.J.H. Brouwers, M. Founti, The behavior of self-compacting concrete containing micro-encapsulated phase change materials, Cem. Concr. Compos. 31(2009)731-743.

[9] J.F. Su, X.Y. Wang, S.B. Wang, Y.H. Zhao, Z. Huang, Fabrication and properties of microencapsulated paraffin/gypsum-matrix building materials for thermal energy storage, Energy Convers. Manage. 55 (2012) 101-107.

[10] T.El Rhafiki, T.Kousksou, A.Allouhi, W.Benomar, H.Zennouhi, A.Jamil, Y.Zeraouli, Numerical analysis of a micro-encapsulated PCM wallboard: Fluxmeter applications, J. Build. Eng.14 (2017) 127-133.

[11]A. D. Catlean, L. Zalewski, A. Joulin, S. Lassue, T. Chartier, Etude thermique comparative de deux mortiers dont l'un contient des matériaux à changement de phase, X^{ème} Colloque Interuniversitaire Franco-Québécois sur la Thermique des Systèmes, 20-22 June 2011, Saguenay.

[12] A. Joulin, L. Zalewski, S. Lassue, H. Naji, Experimental investigation of thermal characteristics of a mortar with or without a micro-encapsulated phase change material, Appl. Therm. Eng. 66 (2014) 171-180.

[13] T. Kousksou, A. Arid, A. Jamil, Y. Zeraouli, Thermal behavior of building material containing microencapsulated PCM, Thermoch. Acta 550 (2012) 42– 47.

[14]T. Kousksou, A. Jamil, Y. Zeraouli, Use of multiple heating rates DSC to determine the specific heat capacity, High Temperatures - High Pressures 39 (2010) 165-179.

[15] S. Drissi, A. Eddhahak, S. Caré, J. Neji, Thermal analysis by DSC of Phase Change Materials, study of the damage effect, J. Build. Eng. 1 (2015) 13–19.

[16] A.Solé, L. Miró, C.Barreneche, I. Martorell, L. F. Cabeza, Review of the T-historymethod to determine thermophysical properties of phase change materials (PCM), Renew. Sustain. Energy Rev. 26 (2013) 425-436.

[17] C. Rathgeber, H. Schmit, L. Miró, L. F. Cabeza, A. Gutierrez, S. N. Ushak, S. Hiebler, Enthalpy-temperature plots to compare calorimetric measurements of phase change materials at different sample scales, J. Energy Storage 15 (2018) 32-38.

[18] C. Rathgeber, L. Miró, L. F. Cabeza, S. Hiebler, Measurement of enthalpy curves of phase change materials via DSC and T-History: When are both methods needed to estimate the behaviour of the bulk material in applications? Thermochimica Acta 596 (2014) 79-88.

[19] G. Höhne, W. Hemminger, H.-J. Flammersheim, Differential Scanning Calorimetry, Springer-Verlag, Berlin, Heidelberg, New York, 2003.

[20] E. Günther, S. Hiebler, H. Mehling, R. Redlich, Enthalpy of phase change materials as a function of temperature: required accuracy and suitable measurement methods, Int. J. Thermophys 30 (2009) 1257–1269.

[21] P. Losada-Pérez, C. S. P. Tripathi, J. Leys, G. Cordoyiannis, C. Glorieux, J.Thoen, Measurements of Heat Capacity and Enthalpy of Phase Change Materials by Adiabatic Scanning Calorimetry, Int. J. Thermophys 32 (2011) 913–924.

[22] G. Albright, M. Farid, S. Al-Hallaj, Development of a model for compensating the influence of temperature gradients within the sample on DSC-results on phase change materials, J. Therm. Anal. Calorim. 101 (2010) 1155–1160.

[23] H.B. Dong, J.D. Hunt, A numerical model for a heat flux DSC: Determining heat transfer coefficients within DSC, Mater. Science Eng. A 413 (2005) 470-473.

[24] M. Mahdaoui, T. Kousksou, S. Blancher, A. AitMsaad, T. El Rhafiki, M. Mouqallid, A numerical analysis of solid–liquid phase change heat transfer around a horizontal cylinder, Appl. Math. Mod. 38 (2014) 1101-1110.

[25] K. Kumarasamy, J. An, J. Yang, E. Yang, Numerical techniques to model conduction dominant phase change systems: A CFD approach and validation with DSC curve, Energy Build. 118 (2016) 240-248.

[26] T. Bouhal, S. Fertahi, T. Kousksou, A. Jamil, CFD thermal energy storage enhancement of PCM filling a cylindrical cavity equipped with submerged heating sources, J. Energy Storage 18 (2018) 360-370.

[27] T. Kousksou, P. Bruel, G. Cherreau, V. Leoussoff, T. El Rhafiki, PCMstorage for solar DHW: From an unfulfilled promise to a real benefit, Sol. Energy 85 (2011) 2033-2040

[28] T. Kousksou, T. El Rhafiki, A. Jamil, P. Bruel, Y. Zeraouli, PCMs inside emulsions: Some specific aspects related to DSC (differential scanning calorimeter)-like configurations, Energy 56 (2013) 175-183.

[29] T. Kousksou, A. Jamil, Y. Zeraouli, Enthalpy and apparent specific heat capacity of the binary solution during the meltingprocess: DSC modeling, Thermoch. Acta 541 (2012) 31-41.

[30] T. Kousksou, A. Jamil, Y. Zeraouli, J. -P. Dumas, Equilibrium liquidus temperatures of binary mixtures from differential scanning calorimetry, Chem. Eng. Science 62 (2007) 6516-6523.

[31] T. Kousksou, A. Jamil, Y. Zeraouli, J. -P. Dumas, DSC study and computer modelling of the melting process in ice slurry, Thermoch. Acta 448 (2006)123-129.

[32] B. Zalba, J.M. Marin, L.F. Cabeza, H. Mehling, Review on thermal energy storage with phase change materials, heat transfer analysis and applications, Appl. Therm. Eng. 23 (2003) 251-83.

[33] M.M. Farid, A.A. Khudair, S.A.K. Razack, S. Al-Hallaj, A review on phase energy storage: materials and applications, Energy Convers. Manag. 45 (2004) 1597-615.

[34] H. Mehling, L.F. Cabeza, Heat and cold storage with PCM: An up to date introduction into basics and applications (2008) Springer.

[35] K. Biswas, Y. Shukla, A. Desjarlais, R. Rawal, Thermal characterization of full-scale PCM products and numerical simulations, including hysteresis, to evaluate energy impacts in an envelope application, Appl. Therm. Eng. 138 (2018) 501-512.

[36] N. Shukla, J. Kosny, DHFMA Method for Dynamic Thermal Property Measurement of PCM-integrated Building Materials, Curr. Sustain. Renew. Energy Rep. 2 (2015) 41-46.

[37] T. El Rhafiki, T. Kousksou, A. Jamil, S. Jegadheeswaran, S.D. Pohekar, Y. Zeraouli, Crystallization of PCMs inside an emulsion: Supercooling phenomenon, Sol. Energy Mater. Sol. Cells 95 (2011) 2588-2597

[38] T. Kousksou, T. El Rhafiki, M. Mahdaoui, P. Bruel, Y. Zeraouli, Crystallization of supercooled PCMs inside emulsions: DSC applications, Sol. Energy Mater. Sol. Cells 107 (2012) 28-36.